either Rab27a or syntaxin 1a lose the targeting activity. The importance of syntaxin 1a in the tethering or docking process of insulin granules also is supported by recent findings from evanescent wave microscopy. Ohara-Imaizumi *et al.* (14) have shown that introduction of the H3 domain of syntaxin 1a into MIN6 cells inhibits new docking events of insulin granules during the glucose stimulation. We have found that the H3 fragment of syntaxin 1a directly binds to granuphilin *in vitro* and that its introduction into MIN6 cells induces a concomitant decrease in newly docked granules and the amount of endogenous granuphilin-syntaxin 1a complex. These results further support the finding that the targeting process of insulin granules is mediated in part by the interaction between granuphilin and syntaxin 1a.

The targeting activity of granuphilin with syntaxin 1a is consistent with the function of other Rab effectors that act as tethering factors in various transport pathways. Two types of tethering factors are proposed: a group of proteins containing coiled-coil structures and several multisubunit complexes (3). Granuphilin is considered to be relatively similar to the former, as its family proteins, exophilins, possess a putative coiled-coil structure at their N termini (21). In terms of its functional role, it is like Rab5 effector EEA1 that is involved in an endosome tethering reaction through the interaction with the target SNARE syntaxin 6 (22). Similarly, the Rab1 effector p115 at the *cis*-Golgi directly binds to syntaxin 5 and GOS28 and stimulates the SNARE complex formation (23). These previous findings along with our own suggest that the tethering/docking process, especially that executed by monomeric Rab effector proteins, may be mediated in part by an interaction with syntaxins.

In contrast to these findings, previous data from *Drosophila* and squid have indicated that syntaxin is not required for the docking of synaptic vesicles (24–26). Neuronal synapses, however, develop a structural and functional specialization of the active zone that imposes a spatial restriction on release, which is not seen in other secretory systems (27). Thus, the machinery for docking may be different between endocrine and neuronal cells. Furthermore, the docking step, in general, relies on relatively weak ultrastructural definition. Even if synaptic vesicles accumulated near the active zones in the absence of syntaxin, they may not be physically and properly docked to them. Without molecular definition, it is difficult to directly demonstrate the docking step, especially in endocrine cells that lack the specialized site. It also is likely that additional factors at the plasma membrane simultaneously play a role in the targeting process.

Recent progress in membrane fusion suggests that Rab proteins and tethering factors play crucial roles in regulating the loose attachment between vesicles and target membranes including initial recognition, whereas SNARE proteins facilitate a tight attachment of two membranes through the formation of a *trans*-SNARE complex (28). All of these factors appear to contribute to the fidelity of membrane fusion. In this context, granuphilin may play a role for the specific targeting of insulin granules to the exocytotic site. This is supported by the finding that granuphilin specifically binds to syntaxin 1a but not to other syntaxins (syntaxin 2 and syntaxin 3) expressed on the plasma membrane in beta cells (11).[3] Recently it has been shown that peripheral syntaxin 1 is concentrated in lipid rafts or in cholesterol-dependent clusters, 200 nm in size, at which secretory vesicles preferentially dock and fuse in PC12 cells (29, 30). Furthermore, Ohara-Imaizumi *et al.* (31) recently have found by evanescent wave microscopic analysis that syntaxin 1 is distributed in numerous separate clusters in the intact plasma membrane of MIN6 cells, where insulin granules were preferentially docked. The targeting site of insulin granules may represent a functionally defined subcompartment of the plasma membrane.

Although the increment of basal insulin secretion caused by granuphilin overexpression may be explained by the peripheral translocation of granules, the profound inhibition of secretagogue-dependent secretion is not well understood. It is of note, however, that regulated secretory pathways should be equipped with machinery such that the activation of the prefusion processes does not automatically lead to an increase in fusion events. It is possible that other molecular players interact with granuphilin and are involved in this phenomenon. In this context, the finding that Munc18-1 interacts with granuphilin *in vitro* and by the mammalian two-hybrid assay (16) is intriguing. Munc18-1 has been shown to act at a prefusion event promoting vesicle docking (32, 33). Furthermore, Munc18-1 exhibits an affinity exclusively to a closed form of syntaxin 1a that is not compatible with the SNARE assembly, and this mode of interaction seems to represent a special adaptation for regulated secretory pathways (34). Thus, the prefusion steps such as docking and priming likely proceed through multiple steps and are closely interconnected with the fusion machinery in regulated secretory pathways. Currently it is unclear whether granuphilin forms a complex with syntaxin 1a and Munc18-1 simultaneously or separately *in vivo*. In any case, granuphilin and Munc18-1 somehow must be dissociated from syntaxin 1a to allow syntaxin 1a to form an open conformation and thus a core complex with other SNARE proteins. In this regard, it should be noted that both syntaxin 1a and Munc18-1 may serve as negative regulators of exocytosis in beta cell lines (5, 35), although both proteins are known to mediate and promote SNARE complex formation. Further studies are required to clarify how the complex formation involving granuphilin, syntaxin 1a, and Munc18-1 is regulated. It also is necessary to identify all other components associated with granuphilin to elucidate the multiple functions of this unique molecule.

Acknowledgments—We thank Dr. K. Nakayama (Kyoto University), Dr. M. Hosaka, H. Yokota-Hashimoto, C. Tanaka, T. Ishizaka, H. Takemura, and M. Hosoi (Gunma University) for generous support.

REFERENCES

1. Jahn, R., Lang, T., and Südhof, T. C. (2003) *Cell* **112**, 519–533
2. Zerial, M., and McBride, H. (2001) *Nat. Rev. Mol. Cell. Biol.* **2**, 107–118
3. Whyte, J. R. C., and Munro, S. (2002) *J. Cell Sci.* **115**, 2627–2637
4. Rorsman, P., and Renström, E. (2003) *Diabetologia* **46**, 1029–1045
5. Nagamatsu, S., Fujiwara, T., Nakamichi, Y., Watanabe, T., Kitahira, H., Sawa, H., and Akagawa, K. (1996) *J. Biol. Chem.* **271**, 1160–1165
6. Plattner, H., Artalejo, A. R., and Neher, E. (1997) *J. Cell Biol.* **139**, 1709–1717
7. Eliasson, L., Renström, E., Ding, W.-G., Proks, P., and Rorsman, P. (1997) *J. Physiol. (Lond.)* **503**, 399–412
8. Olofsson, C. S., Göpel, S. O., Barg, S., Galvanovskis, J., Ma, X., Salehi, A., Rorsman, P., and Eliasson, L. (2002) *Pflügers Arch.* **444**, 43–51
9. Wang, J., Takeuchi, T., Yokota, H., and Izumi, T. (1999) *J. Biol. Chem.* **274**, 28542–28548
10. Yi, Z., Yokota, H., Torii, S., Aoki, T., Hosaka, M., Zhao, S., Takata, K., Takeuchi, T., and Izumi, T. (2002) *Mol. Cell. Biol.* **22**, 1858–1867
11. Torii, S., Zhao, S., Yi, Z., Takeuchi, T., and Izumi, T. (2002) *Mol. Cell. Biol.* **22**, 5518–5526
12. Pouli, A. E., Emmanouilidou, E., Zhao, C., Wasmeier, C., Hutton, J. C., and Rutter, G. A. (1998) *Biochem. J.* **333**, 193–199
13. Hosaka, M., Watanabe, T., Sakai, Y., Uchiyama, Y., and Takeuchi, T. (2002) *Mol. Biol. Cell* **13**, 3388–3399
14. Ohara-Imaizumi, M., Nakamichi, Y., Nishiwaki, C., and Nagamatsu, S. (2002) *J. Biol. Chem.* **277**, 50805–50811
15. Ohara-Imaizumi, M., Nakamichi, Y., Tanaka, T., Katsuta, H., Ishida, H., and Nagamatsu, S. (2002) *Biochem. J.* **363**, 73–80
16. Coppola, T., Fantz, C., Perret-Menoud, V., Gattesco, S., Hirling, H., and Regazzi, R. (2002) *Mol. Biol. Cell* **13**, 1906–1915
17. Zhao, S., Torii, S., Yokota-Hashimoto, H., Takeuchi, T., and Izumi, T. (2002) *Endocrinology* **143**, 1817–1824
18. Kee, Y., Lin, R. C., Hsu, S.-C., and Scheller, R. H. (1995) *Neuron* **14**, 991–998
19. Ohara-Imaizumi, M., Nakamichi, Y., Tanaka, T., Ishida, H., and Nagamatsu, S. (2002) *J. Biol. Chem.* **277**, 3805–3808
20. Izumi, T., Gomi, H., Kasai, K., Mizutani, S., and Torii, S. (2003) *Cell Struct. Funct.* **28**, 465–474
21. Nagashima, K., Torii, S., Yi, Z., Igarashi, M., Okamoto, K., Takeuchi, T., and Izumi, T. (2002) *FEBS Lett.* **517**, 233–238

22. Simonsen, A., Gaullier, J.-M., D'Arrigo, A., and Stenmark, H. (1999) *J. Biol. Chem.* **274,** 28857–28860
23. Shorter, J., Beard, M. B., Seemann, J., Dirac-Svejstrup, A. B., and Warren, G. (2002) *J. Cell Biol.* **157,** 45–62
24. Broadie, K., Prokop, A., Bellen, H. J., O'Kane, C. J., Schulze, K. L., and Sweeney, S. T. (1995) *Neuron* **15,** 663–673
25. O'Connor, V., Heuss, C., De Bello, W. M., Dresbach, T., Charlton, M. P., Hunt, J. H., Pellegrini, L. L., Hodel, A., Burger, M. M., Betz, H., Augustine, G. J., and Schäfer, T. (1997) *Proc. Natl. Acad. Sci. U. S. A.* **94,** 12186–12191
26. Marsal, J., Ruiz-Montasell, B., Blasi, J., Moreira, J. E., Contreras, D., Sugimori, M., and Llinás, R. (1997) *Proc. Natl. Acad. Sci. U. S. A.* **94,** 14871–14876
27. Rosenmund, C., Rettig, J., and Brose, N. (2003) *Curr. Opin. Neurobiol.* **13,** 509–519
28. Söllner, T. H. (2003) *Mol. Membr. Biol.* **20,** 209–220
29. Chamberlain, L. H., Burgoyne, R. D., and Gould, G. W. (2001) *Proc. Natl. Acad. Sci. U. S. A.* **98,** 5619–5624
30. Lang, T., Bruns, D., Wenzel, D., Riedel, D., Holroyd, P., Thiele, C., and Jahn, R. (2001) *EMBO J.* **20,** 2202–2213
31. Ohara-Imaizumi, M., Nishiwaki, C., Kikuta, T., Kumakura, K., Nakamichi, Y., and Nagamatsu, S. (2004) *J. Biol. Chem.*, **279,** 8403–8408
32. Voets, T., Toonen, R. F., Brian, E. C., de Wit, H., Moser, T., Rettig, J., Südhof, T. C., Neher, E., and Verhage, M. (2001) *Neuron* **31,** 581–591
33. Weimer, R. M., Richmond, J. E., Davis, W. S., Hadwiger, G., Nonet, M. L., and Jorgensen, E. M. (2003) *Nat. Neurosci.* **6,** 1023–1030
34. Rizo, J., and Südhof, T. C. (2002) *Nat. Rev. Neurosci.* **3,** 641–653
35. Zhang, W., Efanov, A., Yang, S.-N., Fried, G., Kölare, S., Brown, H., Zaitsev, S., Berggren, P.-O., and Meister, B. (2000) *J. Biol. Chem.* **275,** 41521–41527

Biochemical and Biophysical Research Communications 318 (2004) 698–703

Functions of pancreatic β cells and adipocytes in bombesin receptor subtype-3-deficient mice

Yoko Nakamichi, Etsuko Wada, Kumiko Aoki, Mica Ohara-Imaizumi, Toshiteru Kikuta, Chiyono Nishiwaki, Satsuki Matsushima. Takashi Watanabe, Keiji Wada, and Shinya Nagamatsu

Reprinted from BIOCHEMICAL AND BIOPHYSICAL RESEARCH COMMUNICATIONS, Vol. 318, No. 3, June 4, 2004

Available online at www.sciencedirect.com
SCIENCE DIRECT®
Biochemical and Biophysical Research Communications 318 (2004) 698–703
BBRC
www.elsevier.com/locate/ybbrc

Functions of pancreatic β cells and adipocytes in bombesin receptor subtype-3-deficient mice☆

Yoko Nakamichi,[a] Etsuko Wada,[b,c] Kumiko Aoki,[b] Mica Ohara-Imaizumi,[a] Toshiteru Kikuta,[a] Chiyono Nishiwaki,[a] Satsuki Matsushima,[d] Takashi Watanabe,[d] Keiji Wada,[b] and Shinya Nagamatsu[a,*]

[a] *Department of Biochemistry (II), Kyorin University School of Medicine, Shinkawa 6-20-2, Mitaka, Tokyo 181-8611, Japan*
[b] *Department of Degenerative Neurological Diseases, National Institute of Neuroscience, National Center of Neurology and Psychiatry, 4-1-1 Ogawahigashi, Kodaira, Tokyo 187-8502, Japan*
[c] *Japan Science and Technology Corporation, 4-1-8 Honmachi, Kawaguchi, Saitama 322-0012, Japan*
[d] *Department of Clinical Pathology, Kyorin University School of Medicine, Shinkawa 6-20-2, Mitaka, Tokyo 181-8611, Japan*

Received 13 April 2004
Available online 30 April 2004

Abstract

We previously reported that mice lacking bombesin receptor subtype-3 (BRS-3) exhibit mild late-onset obesity and glucose intolerance [Nature 390 (1997) 160]. To examine the mechanism by which glucose intolerance is developed in these mice, we studied insulin release and proinsulin biosynthesis in isolated pancreatic islets and glucose uptake and facilitative glucose transporter (GLUT)-4 translocation in adipose tissues. Although islet insulin contents and the size and number of islets of Langerhans in BRS-3-deficient mice decreased, there was no difference in glucose-stimulated insulin release and proinsulin biosynthesis between BRS-3-deficient and wild-type control mice. In contrast, adipose tissues exhibited a marked difference: the uptake of [^{14}C]2-deoxy-D-glucose by adipocytes isolated from BRS-3-deficient mice was not stimulated by 10^{-7} M insulin addition, and membrane fractionation analysis showed that GLUT4 was barely detected in the fraction of plasma membrane in BRS-3-deficient mice in the presence of 10^{-7} M insulin. Quantitative reverse transcription-PCR (RT-PCR) showed that mRNA levels of GLUT4, insulin receptor, insulin receptor substrate (IRS)-1 and IRS-2, syntaxin 4, SNAP23, and VAMP-2 in adipose tissues of BRS-3-deficient mice were unchanged compared with those in wild-type control mice. We concluded that impaired glucose metabolism observed in BRS-3-deficient mice was mainly caused by impaired GLUT4 translocation in adipocytes.

Keywords: Bombesin receptor subtype-3-deficient mouse; Pancreatic islet; Insulin; Adipocyte; Glucose transport; GLUT4

Bombesin is a tetradecapeptide originally purified from the skin of the European frog *Bombina bombina* [1]. In mammals, the bombesin-like peptide has a wide spectrum of physiological effects [2,3]. Three subtypes of the bombesin-like peptide receptor have been reported, each belonging to the G-protein-coupled receptor (GPCR) family. Two subtypes, gastrin-releasing peptide receptor (GRP-R) and neuromedin B receptor (NMB-R), have been well characterized. GRP-R [4,5] has a high affinity for gastrin-releasing peptide (GRP) whereas NMB-R [6,7] has a high affinity for neuromedin B (NMB). The third type BRS-3 is an orphan G-protein-coupled receptor that exhibits about 50% homology to GRP-R and NMB-R [8,9].

BRS-3 mRNA is expressed in the hypothalamus, the region of the brain primarily responsible for the regulation of food intake [10–12], although the specific ligand for BRS-3 is still unclear. We previously reported

☆ *Abbreviations:* ELISA, enzyme-linked immunosorbent assay; KRB, Krebs–Ringer buffer; PCR, polymerase chain reaction; SDS, sodium dodecyl sulfate; PAGE, polyacrylamide gel electrophoresis; VAMP-2, vesicle associated membrane protein-2; GLUT, facilitative glucose transporter; GRP-R, gastrin-releasing peptide receptor; NMB-R, neuromedin B receptor.

* Corresponding author. Fax: +81-422-47-5538.
E-mail address: shinya@kyorin-u.ac.jp (S. Nagamatsu).

0006-291X/$ - see front matter © 2004 Elsevier Inc. All rights reserved.
doi:10.1016/j.bbrc.2004.04.081

that mice lacking functional BRS-3 developed mild obesity associated with impairment of glucose metabolism [13], suggesting that BRS-3 is involved in either insulin release from pancreatic β cells or glucose transport in the adipocytes. In this study, to examine the impaired glucose metabolism in vivo, we studied the insulin release and insulin biosynthesis in pancreatic islets and the glucose uptake and GLUT4 translocation in adipose cells of BRS-3-deficient mice.

Materials and methods

Animals. Male BRS-3-deficient mice [13] and male wild-type control littermates were used at the age of 12 weeks. The mice were given free access to food and water until the start of the experiments.

Islet isolation, insulin release, and proinsulin biosynthesis. Pancreatic islets were isolated by collagenase digestion as described previously [14]. For insulin-release experiments, islets were preincubated for 1 h in Krebs–Ringer buffer (KRB) containing 2.2 mM glucose and then challenged by 22 mM glucose for 30 min. For measurements of insulin content, insulin was extracted with acid–alcohol from islets. The aliquots of the media and cell extracts were analyzed by enzyme-linked immunosorbent assay (ELISA) as described previously [14]. Proinsulin biosynthesis experiments were essentially performed as described previously [14]. Briefly, after islets were labeled with 100 μCi [^{3}H]leucine (Amersham–Pharmacia Biotech, Buckinghamshire, UK) for 30 min, they were lysed and immunoprecipitated with guinea pig anti-insulin antibody (Dakocytomation, Denmark).

Immunohistochemistry. Pancreatic tissues were fixed and embedded in Oct compounds, and frozen sections were cut with a cryostat as described previously [15]. For insulin staining, the primary antibody was monoclonal anti-insulin antibody (1:1000; Sigma, St. Louis, MO, USA) and the secondary antibody was FITC-conjugated anti-mouse IgG antibody. The sections were examined by confocal laser-scanning microscopy (Carl Zeiss, Jena, Germany).

Adipocyte glucose transport. Adipocytes were isolated from epididymal fat pads by collagenase digestion essentially based on the method of Rodbell [16]. Isolated adipocytes were incubated with various concentrations of insulin (0, 10^{-10}, 10^{-9}, 10^{-8}, and 10^{-7} M) for 60 min at room temperature (24 °C). [U-^{14}C]2-deoxyglucose was added for 15 min with 0.1 mM 2-deoxy-D-glucose at 24 °C, and the reaction was terminated by separating cells from media by spinning the suspension through dinonyl phthalate oil [17].

GLUT4 translocation. Isolated adipocytes were incubated in the absence or presence of insulin (10^{-7} M) for 30 min at 37 °C. At the end of incubation, adipocytes were homogenized and solubilized, 300 μl of Tris buffer (25 mM Tris–HCl, 150 mM NaCl, and 5 mM EDTA, pH 7.4), containing 10% sucrose, 1% Triton X-100, 1 mM DTT, 1 mM phenylmethylsulfonyl fluoride, 1 mg/ml leupeptin, and 1 mg/ml antipain on ice for 30 min. Subcellular fractionation was performed with 350-μl steps each of 35%, 30%, 25%. 20%, and 0% Optiprep as described previously [18]. The fractions were collected and protein concentrations of each fraction were determined. The same amounts of each fraction were subjected to SDS–PAGE and analyzed by immunoblotting with anti-GLUT4 antibody as described previously [15]. For the analysis of immunoblotting of total cell lysates, the protein bands were scanned and analyzed with NIH Image (National Institutes of Health, Bethesda, MD). The data of intensities were then normalized to these respective protein concentrations, and the data were expressed as a percentage of the mean value in control mouse adipocytes.

Quantitative mRNA analysis by real-time PCR. mRNA gene expression levels were determined by SYBR Green-based real-time quantitation RT-PCR essentially as described previously [19,20]. cDNA was synthesized from total RNA isolated from adipose tissue using random hexamer primer; and SYBR green-based real-time quantitative RT-PCR was performed (applied Biosystems 7700 sequence detection system) in 1× SYBR green master mix using specific primers designed with Primer Express Software (Applied Biosystems). For standardization and quantification, β-actin or glyceraldehyde-3-phosphate dehydrogenate (GAPDH) was amplified simultaneously as described previously [20].

Results and discussion

Studies using pancreatic β cell

Because mice lacking functional BRS-3 develop the impairments of glucose tolerance and insulin tolerance as described [13], we intended to characterize the functions of both pancreatic β cells and adipose cells in this study. First, we studied both insulin secretion and proinsulin biosynthesis in pancreatic β cells. Fig. 1A shows the glucose responsiveness of insulin release from islets of BRS-3-deficient and wild-type control mice. There was no statistical difference among levels of insulin release induced by all values of glucose (from 2.2 to 22 mM). This finding is interesting when compared with the findings of in vivo studies, because we observed the hyper-insulin responsiveness in BRS-3-deficient mice after oral glucose administration in vivo [13]. At present,

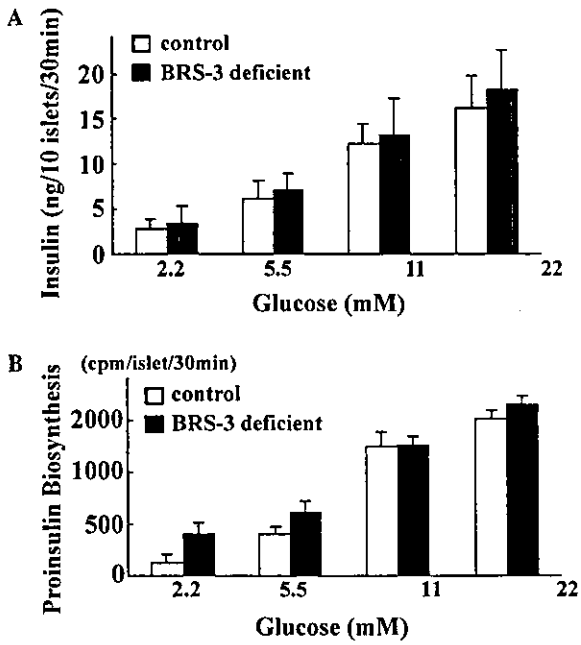

Fig. 1. Comparison of glucose-stimulated insulin release and proinsulin biosynthesis from isolated islets in 12-week-old BRS-3-deficient and wild-type control mice. Mouse islets were isolated and preincubated with 2.2 mM glucose for 1 h. (A) Insulin release. After islets were stimulated with 2.2, 5.5, 11, or 22 mM glucose for 1 h, IRI in the media was measured. (B) Proinsulin biosynthesis. Proinsulin biosynthesis was measured by determining the incorporation of [^{3}H]leucine into anti-insulin-antibody-immunoprecipitable material.

the precise reason for the discrepancy is unknown, but there are some possible explanations. Insulin release in vivo is regulated by several factors other than glucose, such as nutrients, various hormones, and neurotransmitters [21–24]. Although the exact ligand for BRS-3 is unknown, because BRS-3 is prominently expressed in brain [10,11], BRS-3 may be present in peripheral neurons, which may affect the neurotransmitter release such as catecholamines from neurons surrounding islets, probably leading to enhance insulin release after food intake in vivo. Furthermore, because insulin release is dependent on the islet–brain axis, neutral effectors associated with the hypothalamus and brain stem cells regulate the insulin release [25]. Therefore, insulin release regulated by neural control in vivo may be disturbed in BRS-3-deficient mice. Thus, it is likely that BRS-3 itself does not have any direct role in insulin release from pancreatic islets.

We then examined the biosynthetic rate of proinsulin by labeling the islets with [^{3}H]leucine. Islets isolated from BRS-3-deficient and control mice were labeled with [^{3}H]leucine in the presence of 2.2, 5.5, 11, and 22 mM glucose, and proinsulin biosynthesis was measured as described previously [14]. As shown in Fig. 1B, there was no difference in proinsulin biosynthesis between BRS-3-deficient and wild-type control mice, and there was no difference observed in proinsulin processing rate among these mice (data not shown). Thus, there were no apparent differences in insulin release and proinsulin biosynthesis in BRS-3-deficient mice compared with those of control mice. However, we found that the insulin content of the islets in BRS-3-deficient mice was significantly lower than that in control mice (75 ± 20 ng/islet in control vs. 25 ± 16 ng/islet in BRS-3-deficient: $p < 0.001$; see Fig. 3). Because islet functions such as insulin release and proinsulin biosynthesis are intact, we thought that there must be some change in the overall morphological structure of the islets of Langerhans.

Therefore, we immunostained the pancreatic sections with anti-insulin antibody. As shown in Fig. 2, there was no difference in insulin-staining pattern and stringency of each islet between BRS-3-deficient and control mice, although the number and size of islets were markedly changed in BRS-3-deficient mice (Fig. 3). We also observed a marked decline in islet number as well as a significant decrease in the average size of the islet in BRS-3-deficient mice (Fig. 3), indicating that BRS-3 may be associated with the growth of islets with either reduced β cell differentiation and growth or increased β cell death. Indeed, the family of bombesin-like peptides functions as growth factors in rat pancreas [26]. However, as BRS-3 mRNA in islets could not be detected by RT-PCR (data not shown), hypothalamic control of differentiation and growth of these mice may be disturbed. Thus, unknown signals originating from

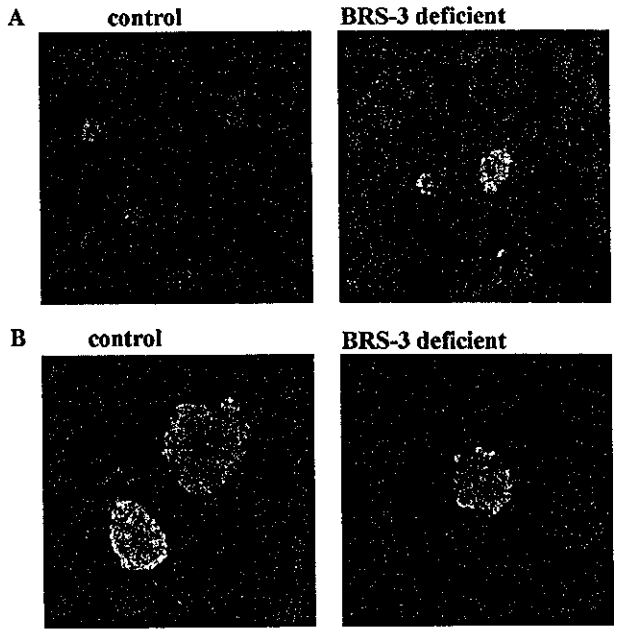

Fig. 2. Islet morphology. Representative images for relative β cell area. (A) Low magnification 4× and (B) high magnification 20×. Left and right panels show the immunostained pancreatic section with anti-insulin antibody in wild-type and BRS-3-deficient mouse pancreas, respectively.

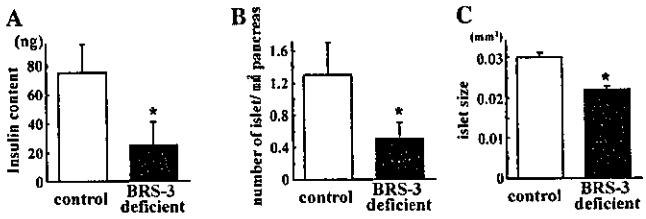

Fig. 3. Islet morphological analysis. (A) Islet insulin content. Insulin was extracted using acid/ethanol for groups of 10 islets and was measured by RIA ($n = 6$). (B) Number of islets per mm^2 pancreas ($n = 6$). (C) Average islet size (mm^2; $n = 6$). *$P < 0.01$ vs. wild-type control.

hypothalamus and related to BRS-3 may regulate the growth of islets, although the molecular basis for the role of such signals in the regulation of β cell mass is presently unknown. Recently, uncoupling protein (UCP)-2 knockout mice show an increase in their β cell mass when eating a high fat diet [27]. In contrast, BRS-3-deficient mice have some association with altered expression of UCP1 in brown adipose tissue [13]. Although it cannot be stated conclusively at present, there may be some relationship between UCP expression and islet growth.

In this study we found that the number and size of islet decreased in BRS-3-deficient mice, whereas insulin release and biosynthesis in response to glucose were preserved. Therefore, this imbalance may cause an

eventual stress on β cells, which may lead to glucose intolerance in vivo.

Studies using adipose cells

We have investigated the insulin-induced glucose uptake from isolated adipocytes. Fig. 4 shows 2-deoxy-glucose uptake in isolated adipocytes in BRS3-deficient and control mice. In control mice, the addition of 10^{-7} M insulin increased 2-deoxy glucose uptake into isolated adipocytes compared with that in the absence of insulin. In BRS-3-deficient mice, however, insulin did not increase glucose uptake into adipocytes at all. These in vitro findings agreed with the observations of in previous vivo studies [13], in which BRS-3-deficient mice exhibited the impaired insulin tolerance, indicating the presence of insulin resistance in adipocytes. In this study, we examined the mechanism behind the lack of insulin effect on adipocyte glucose uptake on the cellular level in BRS-3-deficient mice.

As GLUT4 is the main membrane protein responsible for insulin-induced glucose uptake [28], we studied the total protein (GLUT4) expression level and intracellular distribution of GLUT4 in adipose tissues. As shown in Figs. 5 and 7, the levels of GLUT4 protein and mRNA in adipocytes of BRS-3-deficient mice were unchanged compared with those in the control; however, the cellular distribution of GLUT4 protein analyzed by immunoblotting using anti-GLUT4 antibody was markedly different between BRS-3-deficient and control adipocytes (Fig. 6). To analyze the GLUT4 translocation induced by insulin, we performed the membrane fractionation using Optiprep. Insulin-stimulated and -unstimulated adipocytes from BRS-3-deficient and control mice were extracted with 1% Triton X-100, adjusted to 40% Optiprep, and layered on the bottom of a density

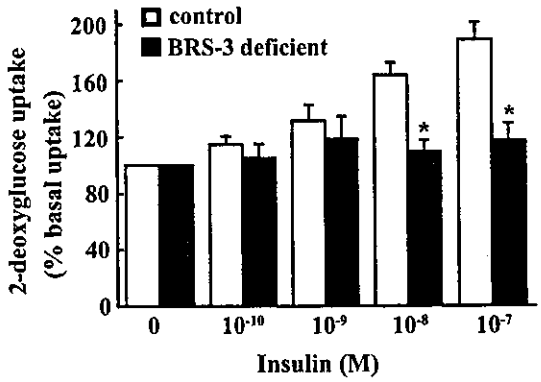

Fig. 4. 2-Deoxy-D-glucose uptake by adipocytes isolated from fat pads of wild-type control and BRS-3-deficient mice. After primary adipocytes were incubated in KRBG buffer for 30 min with various concentrations of insulin, [^{14}C]2-deoxy-D-glucose was added and incubated for 15 min with 0.1 mM of 2-deoxy-D-glucose. The reaction was terminated by separating cells from media by spinning the suspension through dinonyl phthalate oil. Radioactivity uptaken into the cells was counted by a liquid scintillation counter. *$P < 0.001$ vs. wild-type control.

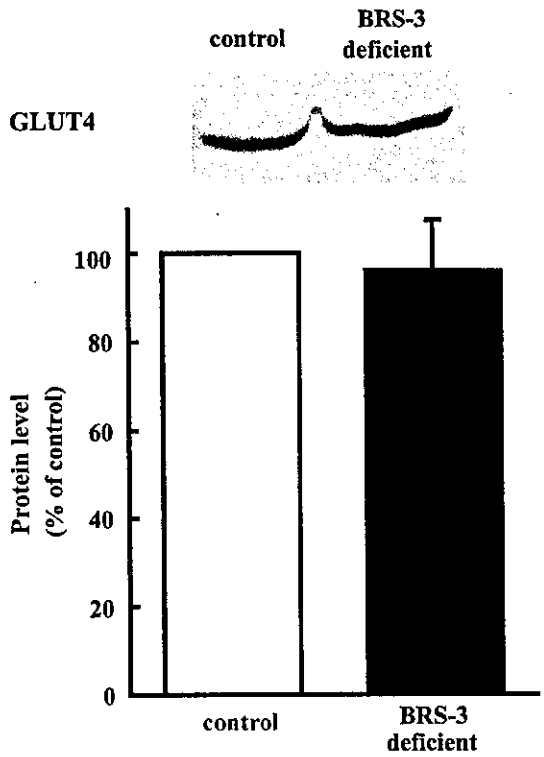

Fig. 5. GLUT4 protein expression level in BRS-3-deficient and wild-type control adipose tissues. Upper panel, immunoblot analysis. Total proteins were extracted from BRS-3-deficient and control adipose tissues, subjected to SDS–PAGE, and immunoblotted with anti-GLUT4 antibody. Protein band was visualized with chemiluminescence detection. (B) Quantitative analysis of protein levels of GLUT4. The levels of GLUT4 bands were determined by imaging analysis, and quantification was carried out by correcting protein concentrations applied to each well. The bars are expressed as a percentage of measurements in the control ($n = 4$).

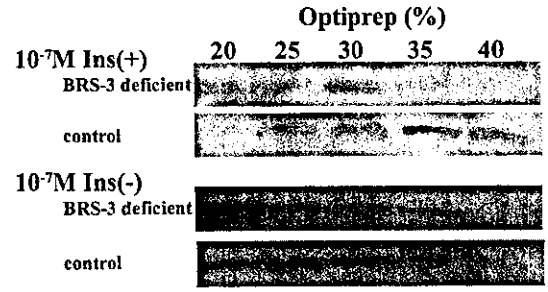

Fig. 6. Intracellular distribution of GLUT4 protein in isolated primary adipocytes. Immunoblotting analysis with anti-GLUT4 antibody of membrane fractions by Optiprep-sucrose gradient was performed using adipocytes isolated from control and BRS-3-deficient mice. After primary adipocytes were incubated with and/or without 10^{-7} M insulin for 30 min, membrane fractionation was carried out as described in Materials and methods. The same protein amounts of each fraction were subjected to SDS–PAGE electrophoresis and immunoblotted with anti-GLUT4 antibody.

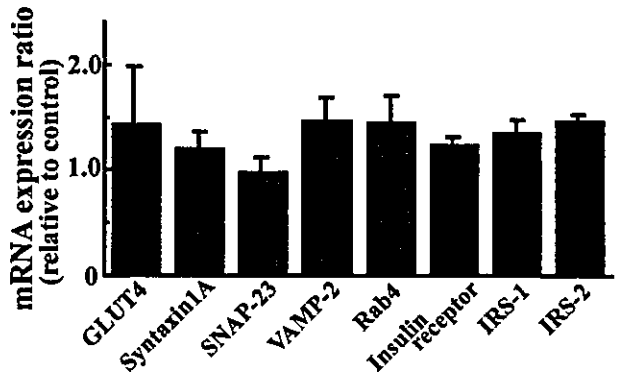

Fig. 7. Gene expression levels in adipose tissues of BRS-3-deficient and wild-type control mice. The expression levels of mRNAs were measured by syber green based real-time PCR and were standardized by expression levels of glyceraldehyde-3-phosphate dehydrogenase (GPDH). The values represent relative expression levels of genes (fold-increase) in the adipose tissues of BRS-3-deficient mice at 3 months of age and were compared with those in age-matched wild-type control mice. Data are means ± SEM ($n = 4$).

gradient. After centrifugation we performed immunoblotting to detect the presence of GLUT4 protein. In insulin-stimulated control adipocytes, a 55 kDa band corresponding to GLUT4 appeared at the bottom of the gradient corresponding to the plasma membrane fraction (Fig. 6, upper panel): in contrast, in insulin-stimulated BRS-3-deficient adipocytes, GLUT4 was not present on this fraction. Thus, membrane fractionation analysis clearly showed that GLUT4 protein is not translocated to the fraction of the plasma membrane by insulin stimulation in BRS-3-deficient adipocytes. An impaired GLUT4 translocation must have caused the lack of insulin-induced glucose uptake. High circulating leptin levels in BRS-3-deficient mice [13] may inhibit the insulin-stimulated glucose uptake [29]. However, because leptin was reported not to affect the GLUT4 translocation [30], this may not be the case.

SNARE proteins, which were originally identified in neuron and contributed to neuronal exocytosis [31,32], are involved in insulin-stimulated trafficking of GLUT4 vesicles in adipocytes [33]. In adipocytes, syntaxin 4, VAMP2, and SNAP-23 are implicated in insulin-regulated GLUT4 trafficking [34]. Therefore, we expected to find impaired expression of these molecules in BRS-3-deficient mice and we measured mRNA expression levels of GLUT4, syntaxin 4, SNAP-23, VAMP-2, and Rab4 in adipose tissues by quantitative RT-PCR. As shown in Fig. 7, we did not observe marked differences in these mRNA expression levels between BRS-3-deficient and control mice. Furthermore, there was no difference in the mRNA expression levels of IR, IRS-1, and IRS-2 among these mice (Fig. 7). Thus, in this context, we cannot reach any definite conclusion about whether the insulin signaling pathway or the exocytotic machinery in GLUT4 translocation may be impaired in BRS-3-deficient mice. Further studies to clarify the mechanism are required.

Conclusion deduced from the two studies

The growth of islets in the pancreas was disturbed by the disruption of BRS-3, but insulin release and biosynthesis were preserved. On the other hand, the GLUT4 translocation system in the adipocytes was impaired by the disruption of BRS-3. Thus, the impairment of glucose metabolism observed in BRS-3-deficient mice may be the result of the impaired GLUT4 translocation in the adipocytes and the stress on β cells.

Acknowledgments

This work was supported by Grants-in-Aid for Scientific Research (C) 14570130 (to M.O.-I.) and (B) 15390108 (to S.N.) from the Japanese Ministry of Education, Culture, Sports, Science, and Technology.

References

[1] A. Anastasi, V. Erspamer, M. Bucci, Alytes Exp. 27 (1971) 166–167.
[2] V. Espamer, Ann. N.Y. Acad. Sci. 547 (1988) 3–9.
[3] T. Lehy, F. Puccio, Ann. N.Y. Acad. Sci. 547 (1988) 255–267.
[4] E.R. Spindel, E. Giladi, P. Brehm, R.H. Goodman, T.P. Segerson, Mol. Endocrinol. 4 (1990) 1956–1963.
[5] J.F. Battey, J.M. Way, M.H. Corjay, H. Shapira, K. Kusano, R. Harkins, J.M. Wu, T. Slattery, E. Mann, R.I. Felman, Proc. Natl. Acad. Sci. USA 88 (1991) 395–399.
[6] M.H. Corjay, D.J. Dobrzanski, J.M. Way, J. Viallet, H. Shapira, P. Worland, E.A. Sausville, J.F. Battey, J. Biol. Chem. 266 (1991) 18771–18779.
[7] E. Wada, J. Way, H. Shapiro, K. Susana, A.M. Lebacq-Verheyden, D. Coy, R. Jensen, J. Battery, Neuron 6 (1991) 421–430.
[8] V. Gorbulev, A. Akhundova, H. Buchner, F. Fahrenholy, Eur. J. Biochem. 208 (1992) 405–410.
[9] Z. Fathi, M.H. Corjay, H. Shapiro, E. Wada, R. Benya, R. Jensen, J. Viallet, E.A. Sausville, J.F. Battey, J. Biol. Chem. 268 (1993) 5979–5984.
[10] H. Ohki-Hamazaki, E. Wada, K. Matsuki, K. Wada, Brain Res. 762 (1997) 165–172.
[11] J.C. Whitley, C. Moove, A.S. Girand, A. Shulkes, J. Mol. Endocrinol. 23 (1999) 107–116.
[12] M.W. Schwartz, S.C. Wood, D. Porte Jr., R.J. Seeley, D.G. Baskin, Nature 404 (2000) 661–671.
[13] H. Ohki-Hamazaki, K. Watase, K. Yamamoto, H. Ogura, M. Yamano, K. Yamada, H. Maeno, J. Imaki, S. Kikuyama, E. Wada, K. Wada, Nature 390 (1997) 165–169.
[14] S. Nagamatsu, Y. Nakamichi, C. Yamamura, S. Matsushima, T. Watanabe, S. Ozawa, H. Furukawa, H. Ishida, Diabetes 48 (1999) 2367–2373.
[15] S. Nagamatsu, T. Watanabe, Y. Nakamichi, C. Yamamura, K. Tsuzuki, S. Matsushima, J. Biol. Chem. 274 (1999) 8053–8060.
[16] M. Rodbell, J. Biol. Chem. 239 (1964) 375–380.
[17] S.W. Cushman, J. Cell Biol. 46 (1970) 326–341.
[18] M. Ohara-Imaizumi, C. Nishiwaki, T. Kikuta, K. Kimakura, Y. Nakamichi, S. Nagamatsu, J. Biol. Chem. 279 (2004) 8403–8408.

[19] R. Wada, C.J. Tifft, R.L. Proia, Proc. Natl. Acad. Sci. USA 97 (2000) 10954–10959.
[20] K. Aoki, Y.-J. Sun, S. Aoki, K. Wada, E. Wada, Biochem. Biophys. Res. Commun. 290 (2002) 1282–1288.
[21] D.G. Pipeleers, F.C. Schuit, P. in't Veld, E. Maes, E.L. Hooghe-Peters, M. Van De Winkel, W. Gept, Endocrinology 117 (1985) 824–833.
[22] F. Schuit, D.G. Pipeleers, Science 232 (1986) 875–877.
[23] K. Moens, H. Heimberg, D. Flamey, P. Huypens, E. Quartier, Z. Ling, D. Pipeleers, S. Gremlich, B. Thorens, F. Schuit, Diabetes 45 (1996) 257–261.
[24] K. Moens, V. Berger, J.-M. Ahn, C.V. Schravendijk, V.J. Hruhy, D. Pipeleers, F. Schuit, Diabetes 51 (2002) 669–675.
[25] F.C. Schuit, P. Huypens, H. Heimberg, D.G. Pipeleers, Diabetes 50 (2001) 1–11.
[26] A. Fleischmann, U. Laderach, H. Friess, M.W. Buechler, J.C. Reubi, Lab. Invest. 80 (2000) 1807–1817.
[27] J.W. Joseph, V. Koshkin, C.Y. Zhang, J. Wang, B.B. Lowell, C.B. Chan, M.B. Wheeler, Diabetes 51 (2002) 3211–3219.
[28] D.F. Burant, W.I. Sivity, H. Fukumoto, T. Kayano, S. Nagamatsu, S. Seino, J.E. Pessin, G.I. Bell, in: C.W. Bardin (Ed.), Recent Progress in Hormone Research, vol. 47, Academic Press, NY, 1991, pp. 349–388.
[29] T. Ishizuka, P. Ernsherger, S. Liu, D. Bedol, T.M. Lehman, R.J. Koletsky, J.E. Freidman, J. Nutr. 128 (1988) 2299–2306.
[30] G. Sweeney, J. Keen, R. Somwar, D. Konrad, R. Garg, A. Klip, Endocrinology 142 (2001) 4806–4812.
[31] T.C. Sadhof, Nature 375 (1995) 645–653.
[32] T. Weber, B.V. Zemelmann, J.A. McNew, B. Westermann, M. Gmach, F. Parlati, T.H. Sollner, J.E. Rothman, Cell 92 (1998) 759–772.
[33] B. Cheatham, A. Volchuk, C.R. Kahn, L. Wang, C.J. Rhodes, A. Klip, Proc. Natl. Acad. Sci. 93 (1996) 15169–15173.
[34] D.C. Thurmond, J.S. Elmendorf, K.J. Coker, S. Okada, J.E. Pessin, in: D. LeRoith, S.I. Taylor, J.M. Olefsky (Eds.), Diabetes Mellitus, second ed., Lippincott Williams and Wilkins, Philadelphia, PA, 2000, pp. 273–279.

Accelerated Publication

THE JOURNAL OF BIOLOGICAL CHEMISTRY
Vol. 279, No. 40, Issue of October 1, pp. 41271–41274, 2004

The Cytokine Interleukin-1β Reduces the Docking and Fusion of Insulin Granules in Pancreatic β-Cells, Preferentially Decreasing the First Phase of Exocytosis*[S]

Received for publication, August 2, 2004, and in revised form, August 13, 2004
Published, JBC Papers in Press, August 18, 2004,
DOI 10.1074/jbc.C400360200

Mica Ohara-Imaizumi‡, Alessandra K. Cardozo§¶, Toshiteru Kikuta‡, Decio L. Eizirik§, and Shinya Nagamatsu‡‖

From the ‡Department of Biochemistry, Kyorin University School of Medicine, 6-20-2 Shinkawa, Mitaka, Tokyo 181-8611, Japan and the §Laboratory of Experimental Medicine, Free University Brussels (ULB), 808 Route de Lennik, CP 618 B-1070 Brussels, Belgium

The prediabetic period in type I diabetes mellitus is characterized by the loss of first phase insulin release. This might be due to islet infiltration mediated by mononuclear cells and local release of cytokines, but the mechanisms involved are unknown. To determine the role of cytokines in insulin exocytosis, we have presently utilized total internal reflection fluorescence microscopy (TIRFM) to image and analyze the dynamic motion of single insulin secretory granules near the plasma membrane in live β-cells exposed for 24 h to interleukin (IL)-1β or interferon (IFN)-γ. Immunohistochemistry observed via TIRFM showed that the number of docked insulin granules was decreased by 60% in β-cells treated with IL-1β, while it was not affected by exposure to IFN-γ. This effect of IL-1β was paralleled by a 50% reduction in the mRNA and the number of clusters of SNAP-25 in the plasma membrane. TIRF images of single insulin granule motion during a 15-min stimulation by 22 mM glucose in IL-1β-treated β-cells showed a marked reduction in the fusion events from previously docked granules during the first phase insulin release. Fusion from newcomers, however, was well preserved during the second phase of insulin release of IL-1β-treated β-cells. The present observations indicate that IL-1β, but not IFN-γ, has a preferential inhibitory effect on the first phase of glucose-induced insulin release, mostly via an action on previously docked granules. This suggests that β-cell exposure to immune mediators during the course of insulitis might be responsible for the loss of first phase insulin release.

Accumulating evidence over the past 30 years suggests that β-cells are destroyed by an autoimmune process in type 1 diabetes mellitus (T1D)[1] (1). The prediabetic period in humans is characterized by the presence of islet cell autoantibodies (2), which seem to have a close correlation with histological evidence of autoimmunity (3). There are already subtle changes in β-cell function during this period, including both disproportionately elevated proinsulin/insulin levels (4, 5) and a preferential loss of the first phase insulin secretion in response to an intravenous glucose challenge (6–9). Of note, β-cell suppression precedes β-cell death in T1D, as suggested by results obtained in islets isolated from prediabetic non-obese diabetic mice (10, 11) or from a patient who died immediately after diagnosis of T1D (12). This initial β-cell functional suppression might be due to exposure to cytokines. Indeed, our previous observations (13) indicate that islet exposure to cytokines under *in vitro* conditions reproduce the disproportionately elevated proinsulin/insulin levels observed in prediabetic patients. Moreover, microarray analysis of purified β-cells or insulin-producing INS-1 cells cultured in the presence of IL-1 β or IL-1β + IFN-γ showed inhibition of the expression of several genes involved in the exocytosis of insulin granules, including SNAP-25, VAMP-2, and Rab3 (14, 15). This raised the intriguing possibility that cytokines could also contribute for the defective first phase insulin release observed in prediabetic patients.

The biphasic kinetics of insulin release is probably explained by the presence of a small population of docked granules, released during the first phase of insulin secretion, and the subsequent arrival of "newcomer" granules targeted to the plasma membrane and released during the second phase of insulin secretion (16, 17). The three SNAREs (*N*-ethylmaleimide-sensitive fusion protein attachment protein receptors), namely SNAP-25, syntaxin 1, and synaptobrevin (VAMP) are expressed in pancreatic β-cells and play a crucial role for granule fusion with the cell membrane (18–20). To better understand the mechanisms involved in insulin granule exocytosis, we have recently developed an approach based on a green fluorescence protein (GFP)-tagged insulin granule system, combined with total internal reflection microscopy (TIRFM) (21). This system allows us to observe the motions of single insulin granules during approach, docking, and fusion with the membrane and also to localize endogenous t-SNAREs such as SNAP-25 and syntaxin-1 in the cell membrane (22, 23). We have presently utilized this system to characterize insulin granule motion in β-cells treated for 24 h with cytokines. The

* This work was supported by Grants-in-aid for Scientific Research (C) 14570130 (MO-I) and (B) 15390108 (SN) and Scientific Research on Priority Areas 16044240 (MO-I) from the Japan Ministry of Education, Culture, Sports, Sciences, and Technology and by grants from the European Foundation for the Study of Diabetes (EFSD)/Novo Nordisk Diabetes Research Fund, Action de Recherche Concertees (ARC) de la Communaute Francaise, Belgium, and the Fonds National de la Recherche Scientifique (FNRS), Belgium. This work has been conducted in collaboration with and partially supported by the Juvenile Diabetes Research Foundation (JDRF) Center for Prevention of β-Cell Destruction in Europe under Grant 4-2002-457. The costs of publication of this article were defrayed in part by the payment of page charges. This article must therefore be hereby marked "*advertisement*" in accordance with 18 U.S.C. Section 1734 solely to indicate this fact.

[S] The on-line version of this article (available at http://www.jbc.org) contains supplemental Quick Time movies S1–S3.

¶ Recipient of a Postdoctoral Fellowship from the JDRF.

‖ To whom correspondence should be addressed. Tel.: 81-422-47-5511 (ext. 3437); Fax: 81-422-47-5538; E-mail: shinya@kyorin-u.ac.jp.

[1] The abbreviations used are: T1D, type 1 diabetes mellitus; GAPDH, glyceraldehyde-3-phosphate dehydrogenase; GFP, green fluorescent protein; IL, interleukin; IFN, interferon; KRB, Krebs-Ringer buffer; RT, reverse transcriptase; SNAP-25, synaptosmal-associated protein of 25 kDa; VAMP, vesicle-associated membrane protein; SNARE, soluble *N*-ethylmaleimide-sensitive fusion protein attachment protein receptor; TIRF, total internal reflection fluorescence; TIRFM, TIRF microscopy.

data obtained suggest that IL-1β reduces the docking/fusion of insulin granules in pancreatic β-cells, preferentially decreasing the first phase of exocytosis, along with a decrease in SNAP-25 mRNA expression and SNAP-25 clusters on the plasma membrane.

EXPERIMENTAL PROCEDURES

Islet Cell Preparation, Adenovirus Infection, and Exposure to Cytokines—Pancreatic islets of Langerhans were isolated from male Wistar rats by collagenase digestion, as described (17). Isolated islets were dispersed in calcium-free Krebs-Ringer buffer (KRB) containing 1 mM EGTA and cultured on fibronectin-coated (Koken Co. Ltd., Tokyo, Japan) high refractive index glass (Olympus, Tokyo, Japan) in RPMI 1640 medium (Invitrogen) supplemented with 10% fetal bovine serum (Invitrogen), 200 units/ml penicillin, and 200 μg/ml streptomycin at 37 °C in an atmosphere of 5% CO_2. For labeling the insulin secretory granules, pancreatic β-cells were infected with recombinant adenovirus Adex1CA insulin-GFP as described previously (17). Two days after infection, they were exposed for 24 h to IL-1β (100 units/ml; kindly provided by Dr. C. W. Reynolds, NCI, Bethesda, MD) and/or IFN-γ (2000 units/ml; Invitrogen, Baesley, Scotland). For determination of mRNA expression (see below) and insulin content, rat pancreatic β-cells were purified by autofluorescence-activated cell sorting, cultured overnight, and exposed for 24 h to IL-1β and/or IFN-γ, and insulin was measured by radioimmunoassay as described previously (14, 24).

Immunohistochemical Analysis—Single cells cultured on high refractive index glass with and/or without cytokines were fixed, made permeable with 2% paraformaldehyde, 0.1% Triton X-100, and processed for immunohistochemistry as described previously (22). They were labeled with monoclonal anti-insulin antibody (Sigma) and anti-SNAP-25 antibody (Wako, Co. Ltd., Osaka, Japan) and then processed with goat anti-mouse IgG conjugated to Alexa Fluor-488 (Molecular Probes, Eugene, OR). Immunofluorescence was detected with TIRFM. This procedure allowed us to evaluate the number of docked insulin granules and SNAP-25 clusters.

TIRF Microscopy for Observing the Immunofluorescence and for Monitoring GFP-tagged Insulin Granule Motion—The Olympus total internal reflection system was used with minor modifications as described previously (21). Briefly, light from an argon laser (488 nm) was introduced to an inverted microscope (IX70, Olympus) through a single-mode fiber and two illumination lenses; the light was focused at the back focal plane of a high aperture objective lens (Apo 100×OHR; NA 1.65, Olympus). To observe the fluorescence image of Alexa Fluor-488, we used a 488-nm laser line and a long pass 515-nm filter. To monitor the motion of the single insulin granules, the adenovirus-infected and cytokine-treated cells on the glass coverslip (Olympus) were mounted in an open chamber and incubated for 30 min at 37 °C in KRB containing 110 mM NaCl, 4.4 mM KCl, 1.45 mM KH_2PO_4, 1.2 mM $MgSO_4$, 2.3 mM calcium gluconate, 4.8 mM $NaHCO_3$, 2.2 mM glucose, 10 mM HEPES (pH 7.4), and 0.3% bovine serum albumin. Cells were then transferred to the thermostat-controlled stage (37 °C), and stimulation with glucose was achieved by addition of 52 mM glucose-KRB into the chamber (final concentration: 22 mM glucose). For observation of GFP, we used a 488-nm laser line for excitation and a 515-nm long pass filter for the barrier. Diodomethane sulfur immersion oil was used to make contact between the objective lens and the coverslip, and the measured penetration depth was about 45 nm.

Acquiring the Images and Analysis—Images were collected by a cooled charge-coupled device camera (Micromax, MMX-512-BFT, Princeton Instruments; operated with Metamorph 4.6, Universal Imaging, Downingtown, PA). Images were acquired every 300 ms. The analyses, including tracking (the single projection of different images) and area calculations were performed using Metamorph software. To analyze the data, fusion events were manually selected, and the average fluorescence intensity of individual granules in a 1 × 1-μm square placed over the granule center was calculated. The number of fusion events was manually counted while looping about 30,000 frame time lapses. Sequences were exported as single TIFF files and further processed using Adobe Photoshop 6.0, or they were converted into Quick Time movies (see supplemental material). This procedure allowed us to dynamically evaluate single insulin granule motion.

mRNA Isolation and RT-PCR—mRNA isolation and RT-PCR were performed as described previously (25). The number of cycles was selected to allow linear amplification of the cDNA under study. For semiquantitative PCR, the housekeeping gene glyceraldehyde-3-phosphate dehydrogenase (GAPDH) was used as control. We have previously shown (26) and confirmed in the present experiments that a 6–24-h exposure to IL-1β and IFN-γ do not affect *GAPDH* mRNA expression in purified β-cells. Thus, *GAPDH* expression was as follows after, respectively, 6 and 24 h treatments (optical density values; means ± S.E. of four experiments): 6 h, control, 8.6 ± 0.5; IL-1β, 8.4 ± 0.8; IFN-γ, 8.5 ± 0.4; IL-1β + IFN-γ, 8.2 ± 0.9; 24 h, control, 6.2 ± 0.6; IL-1β, 7.1 ± 0.8; IFN-γ, 6.1 ± 0.8; IL-1β + IFN-γ, 6.7 ± 1.2. The primer sequences were as follows: *GAPDH*, 5′ TCC CTC AAG ATT GTC AGC AA 3′ (forward) and 5′ AGA TCC ACA ACG GAT ACA TT 3′ (reverse); SNAP-25, 5′ GAT GTC GGC ATC AGG ACT TT 3′ (forward) and 5′ GAG TCA GCC TTC TCC ATG AT 3′ (reverse); and VAMP-2, 5′ TCA GCA CTT AAG TCC CTG AG 3′ (forward) and 5′ CGT AGA CGA TAC GTT ATC GG 3′ (reverse).

Statistical Analysis—Data are presented as means ± S.E., and comparison between groups was performed by *t* test or by Wilcoxon Rank Sum Test or by analysis of variance followed by Fisher's test and regression analysis.

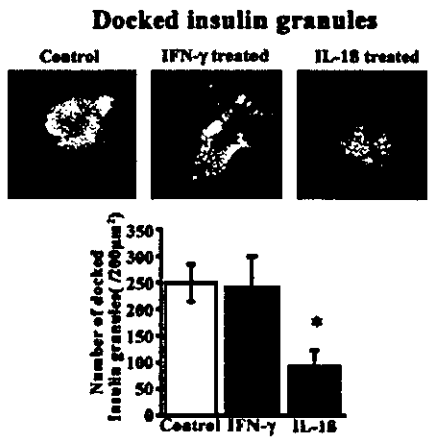

FIG. 1. **Histochemical study of insulin granules docked to the plasma membrane.** The *upper panel* shows the typical TIRF images of docked insulin granules in control, IL-1β, or IFN-γ-treated β-cells. Pancreatic β-cells were prepared from Wistar rats, exposed to IL-1β or IFN-γ for 24 h, and then immunostained for insulin. The *lower panel* shows the number of insulin granules morphologically docked to the plasma membrane. Individual fluorescent spots shown in TIRF images were manually counted per 200 μm^2; $n = 11$ cells. *, $p < 0.0001$ *versus* control.

RESULTS AND DISCUSSION

IL-1β, but Not IFN-γ, Reduced the Number of Insulin Granules Docked to the Plasma Membrane—To examine the docking status of insulin granules by cytokines exposure, rat primary pancreatic β-cells were exposed to IL-1β or IFN-γ for 24 h, immunostained with anti-insulin antibody, and then examined by TIRF microscopy. TIRF imaging depicts the single insulin granules docked to the plasma membrane, enabling accurate docked insulin granule counting (17). We defined "docked granule" when the vesicle was located within 100 nm of the plasma membrane as reported somewhere (27). As shown in Fig. 1, the number of docked insulin granules in β-cells treated with IL-1β was markedly decreased (248.9 ± 35.1 per 200 μm^2 in control *versus* 92.6 ± 31.0 in IL-1β; $n = 11$ cells; $p < 0.0001$), but there was no difference between IFN-γ-treated (240.6 ± 59.1 per 200 μm^2) and control cells. We have shown previously that a 24-h exposure of β-cells to IL-1β does not affect insulin content and cell viability (24, 28, 29), and in experiments performed in parallel with the determinations of mRNA expression (see below), we observed that a 24-h exposure to IL-1β + IFN-γ also failed to affect β-cell insulin content: control β-cells, 28 ± 9 ng of insulin/10^6 cells; IL-1β + IFN-γ, 25 ± 5 ng of insulin/10^6 cells ($n = 4$). Thus, the decreased number of docked insulin granules in IL-1β-treated β-cells is not due to a decrease in insulin content but is probably caused by IL-1β-mediated impairment of insulin granule docking.

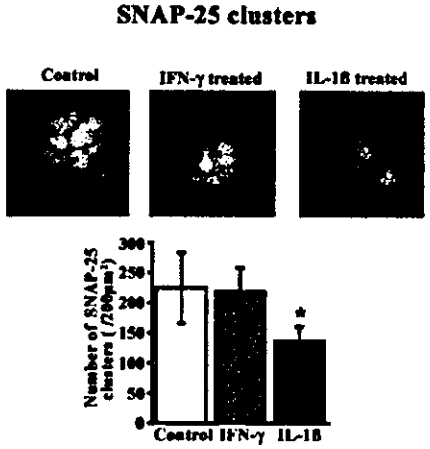

FIG. 2. **TIRF images and the quantitative analysis of SNAP-25 clusters on the β-cell plasma membrane.** Pancreatic β-cells were treated as described the legend of Fig. 1 and immunostained for SNAP-25. The *upper panel* shows the typical TIRF images of SNAP-25 clusters on the plasma membrane. The *lower panel* shows the number of SNAP-25 clusters per 200 μm^2 counted using TIRF images; $n = 14$ cells. *, $p < 0.0001$ *versus* control.

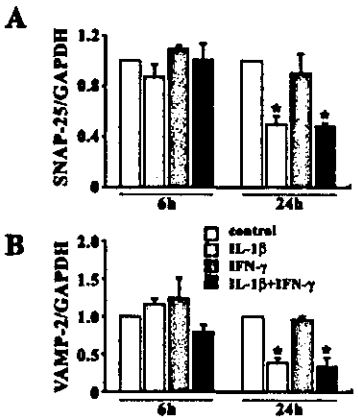

FIG. 3. **RT-PCR analysis of SNAP-25 (*A*) and VAMP-2 (*B*) mRNA expression.** Rat β-cells (10^5 cells/condition) were exposed for 6 or 24 h to control condition, IL-1β (50 units/ml), IFN-γ (1000 units/ml)), or IL-1β + IFN-γ. After these time points, the cells were harvested, mRNA extracted, and the RT-PCR performed with the equivalent of 1.5×10^3 cells. PCR band intensities were expressed as optical density corrected for *GAPDH* expression. The data are presented as percentage of the respective controls, which received an arbitrary value 1 in each experiment; $n = 4$ experiments. *, $p < 0.01$ *versus* control group.

IL-1β Decreased SNAP-25 Clusters and SNAP-25 mRNA Expression—It is well known that SNARE proteins play an important role in docking/fusion of insulin granules (18–20), and we have recently demonstrated by TIRF imaging analysis that syntaxin 1 and SNAP-25 are distributed in numerous separate clusters in the intact plasma membrane of MIN6 cells and rat primary pancreatic β-cells (22, 23). Against this background, we presently analyzed quantitatively and spatially the expression of SNAP-25 protein on the plasma membrane. As shown in Fig. 2, the number of SNAP-25 clusters on the plasma membrane of pancreatic β-cells treated with IL-1β decreased to about half of the control levels (225.1 ± 58.8 per 200 μm^2 in control *versus* 136.1 ± 24.3 per 200 μm^2 in IL-1β; $p < 0.0001$, $n = 14$ cells). In contrast, IFN-γ treatment did not affect the number of SNAP-25 clusters (218.7 ± 40.4 per 200 μm^2). In line with these observations, a 24-h exposure of β-cells to IL-1β, but not to IFN-γ, induced a 50% decrease in SNAP-25 mRNA expression (Fig. 3*A*). This inhibitory effect of IL-1β was not

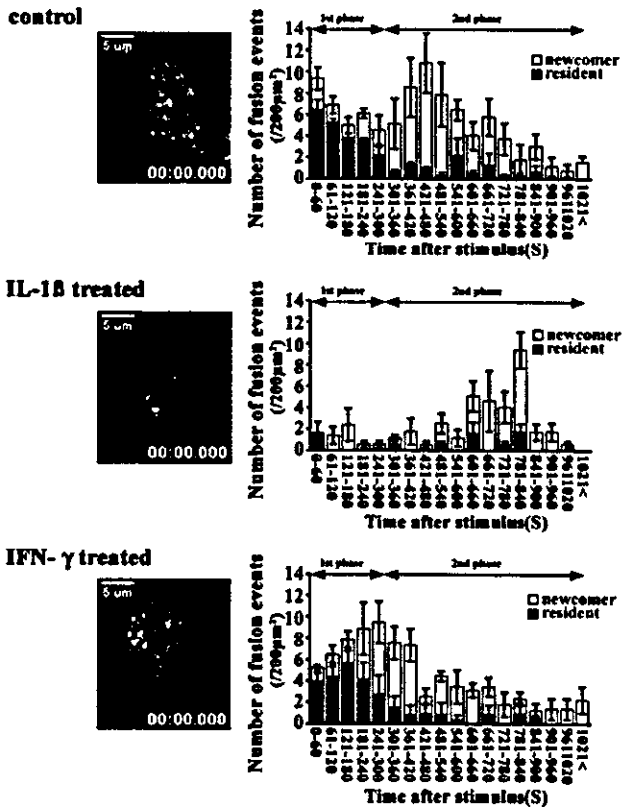

FIG. 4. **TIRF images and analysis of single GFP-labeled insulin granule motion.** After normal rat pancreatic β-cells were prepared and cultured as described under "Experimental Procedures," they were infected with Adex1CA insulin-GFP. Two days later, infected cells were exposed to IL-1β and IFN-γ for 24 h. On the experimental day, cells were preincubated with KRB, 2.2 mM glucose for 30 min and then transferred to the thermostat-controlled stage and stimulated with 22 mM glucose. The real-time motion of GFP-labeled insulin granules was imaged close to the plasma membrane (300-ms intervals) (see movies: S1 (control), S2 (IL-1β-treated), S3 (IFN-γ-treated cells)). The represented pictures next to the histogram are images before stimulation. The *graph* shows the histogram of the number of fusion events (per 200 μm^2) at 60-s intervals after stimulation. The *black column* shows the fusion from previously docked granules (resident), while the *open column* indicates that from newcomers.

potentiated by the concomitant presence of IFN-γ (Fig. 3*A*). Similarly, IL-1β treatment decreased VAMP-2 mRNA expression, and this inhibitory effect was also not potentiated by IFN-γ (Fig. 3*B*). Thus, IL-1-β treatment reduced SNAP-25 mRNA expression and the number of SNAP-25 clusters, along with the reduction of docked insulin granules. The exact molecular regulation of the different stages of membrane fusion still remains to be clarified and it is difficult to precise the mechanism by which the IL-1β-induced reduction in SNAP-25 mRNA and protein expression might lead to a preferential decrease in granule docking. Nevertheless, it appears that SNAP-25 plays a crucial role in the docking status (23), and it has been reported recently that SNAP-25 is a strictly required molecule in evoked fusion events (30, 31). Of note, IL-1β inhibits the expression of mRNAs encoding for other proteins potentially involved in this process, including VAMP-2 (present data) and Rab3 (14, 15). Additional experiments are now required to clarify how these diverse effects of IL-1β will culminate in the observed modifications of exocytosis.

TIRF Imaging Analysis of Single Insulin Granule Motion—Since the frequency of granule fusion and the demand for granules change continuously in response to external signals, releasable granules must be replenished in concert with fusion

events. The present observations suggest that IL-1β affects at least one crucial step in this delicate balance, namely the docking of insulin granules. In the present study, we explored the effects of IL-1β on insulin granule fusion at the cellular level. To obtain a dynamic TIRF image of insulin exocytosis from cytokine-treated β-cells, rat primary β-cells were first infected with Adex1CA insulin-GFP to label the insulin granules and then exposed to IL-1β or IFN-γ for 24 h. Fig. 4 shows the real-time TIRF images of a single insulin granule motion when stimulated by 22 mM glucose for 15 min (for control, see movie S1). As shown in the histogram of number of fusion events per min (Fig. 4; Control), the fusing granules originated mostly from previously docked granules during the first phase of glucose-stimulated insulin release (0–5min), while during the second phase(>5min) those fusing granules arose mostly from newcomers as previously described (17, 21). This pattern was, however, modified following exposure of β-cells to IL-1β (Fig. 4; IL-1β-treated; see movie S2). There were rare fusion events during the first phase (movie S2), and the histogram of fusion events (Fig. 4) indicates a clear reduction in the number of fusion events during the first phase. Moreover, there was a marked reduction in the fusion from previously docked granules in IL-1β-treated β-cells, while the fusion from newcomers during the later second phase was preserved. We quantitatively analyzed the data shown in Fig. 4. The results showed that the total number of fusion events in IL-1β-treated cells during the first phase (0–5 min) was significantly decreased (27.3 ± 6.9 in control *versus* 6.5 ± 5.2 in IL-1β-treated cells in 0–300 s, $n = 4, p < 0.005$). Remarkably, very few fusion events occurred from previously docked granules in IL-1β-treated cells (19.1 ± 4.2 in control *versus* 1.6 ± 1.1 in IL-1β-treated cells, $n = 4, p < 0.0005$). On the other hand, during the second phase (>5 min), there was no significant difference of total number of fusion events between control and IL-1β-treated cells despite a trend for reduced values in IL-1β-treated cells (control, 65.2 ± 21.0: IL-1β-treated, 34.4 ± 18.1 during 301–1020 s, $n = 4$). Of note, IFN-γ-treated β-cells have a similar TIRF image as compared with that of controls (see movie S3). Although the number of fusion events in IFN-γ-treated β-cells appeared to be increased during the first phase (Fig. 4), there was no statistical difference in the number of total fusion events between control and IFN-γ-treated β-cells. There was also no significant difference of total number of fusion events during the second phase (65.2 ± 21.0 in control *versus* 48.5 ± 9.1 in IFN-γ-treated cells during 301–1020 s, $n = 4$). As a whole, our observations suggest that IL-1β has a preferential inhibitory effect on the first phase of glucose-induced insulin release, mostly via an action on previously docked granules. Based on our present data, it is conceivable that IL-1β treatment decreases the number of SNAP-25 clusters, leading to the decreased number of docked insulin granules and thus contributing for a loss of first phase insulin exocytosis. Of note, while there was a 60% reduction of docked insulin granules in IL-1β-treated β-cells, the reduction in fusion events was even more marked (nearly 90%), suggesting that IL-1β may also impair the priming step from docking to fusion.

In conclusion, the present observations suggest that IL-1β has a preferential inhibitory effect on the first phase of glucose-induced insulin release, mostly via an action on previously docked granules. This bears similarity to the pattern of insulin release observed in prediabetic subjects. The present data, together with our previous observations (13), raise the possibility that β-cell exposure to immune mediators during the course of insulitis is responsible for the key metabolic modifications observed in this period, namely disproportionately elevated proinsulin release and loss of first phase insulin release.

REFERENCES

1. Gale, E. A. M. (2001) *Diabetes* **50,** 217–226
2. Notkins, A. L. (2002) *J. Biol. Chem.* **277,** 43545–43548
3. Imagawa, A., Hanafusa, T., Tamura, S., Moriwaki, M., Itoh, N., Yamamoto, K., Iwahashi, H., Yamagata, K., Waguri, M., Nanmo, T., Uno, S., Nakajima, H., Nanba, M., Kawata, S., Miyagawa, J., and Matsuzawa, Y. (2001) *Diabetes* **50,** 1269–1273
4. Roder, M. E., Knip, M., Hartling, S. G., Karjalainen, J., Akerblom, H. K., and Binder, C. (1994) *J. Clin. Endocrinol. Metab.* **79,** 1570–1575
5. Spinas, G. A., Snorgaard, O., Hartling, S. G., Oberholzer, M., and Berger, W. (1992) *Diabetes Care* **1,** 632–637
6. Srikanta, S., Ganda, O. P., Jackson, R. A., Gleason, R. E., Kaldany, A., Garoboy, M. R., Milford, E. L., Carpenter, C. B., Soeldner, J. S., and Eisenbarth, G. S. (1983) *Ann. Int. Med.* **99,** 320–326
7. Srikanta, S., Ganda, O. P., Rabizadeh, A., Soeldner, J. S., and Eisenbarth, G. S. (1985) *N. Engl. J. Med.* **313,** 461–464
8. Chase, H. P., Voss, M. A., Butler-Simon, N., Hoops, S., O'Brien, D., and Dobersen, M. J. (1987) *J. Pediatr.* **111,** 807–812
9. Vardi, P., Crisa, L., Jackson, R. A., and coauthors (1991) *Diabetologia* **34,** 93–102
10. Strandell, E., Eizirik, D. L., and Sandler, S. (1990) *J. Clin. Invest.* **85,** 1944–1950
11. Strandell, E., Sandler, S., Boitard, C., and Eizirik, D. L. (1992) *Diabetologia* **35,** 924–931
12. Conget, I., Fernandez-Alvarez, J., Ferrer, J., Sarri, Y., Novials, A., Somoza, N., Pujol-Borrell, R., Casamitjana, R., and Gomis, R. (1993) *Diabetologia* **36,** 358–360
13. Hostens, K., Pavlovic, D., Zambre, Y., Ling, Z., Van Schravendijk, C., Eizirik, D. L., and Pipeleers, D. G. (1999) *J. Clin. Invest.* **104,** 67–72
14. Cardozo, A. K., Kruhoffer, M., Leeman, R., Orntoft, T., and Eizirik, D. L. (2001) *Diabetes* **50,** 909–920
15. Kutlu, B., Cardozo, A. K., Darville, M. I., Kruhoffer, M., Magnusson, N., Orntoft, T., and Eizirik, D. L. (2003) *Diabetes* **52,** 2701–2719
16. Rorsman, P., Eliasson, L., Renstrom, E., Gromada, J., Barg, S., and Gopel, S. (2000) *News Physiol. Sci.* **15,** 72–77
17. Ohara-Imaizumi, M., Nishiwaki, C., Kikuta, T., Nagai, S., Nakamichi, Y., and Nagamatsu, S. (2004) *Biochem. J.* **381,** 13–18
18. Jacobsson, G., Bean, A. J., Scheller, R. H., Juntti-Berggren, L., Deeney, J. T., Berggren, P.-O., and Meister, B. (1994) *Proc. Natl. Acad. Sci. U. S. A.* **91,** 12487–12491
19. Wheeler, M. B., Sheu, L., Ghai, M., Bouquillon, A., Grondin, G., Weller, U., Beaudoin, A. R., Bennett, M. K., Trimble, W. S., and Gaisano, H. Y. (1996) *Endocrinology* **137,** 1340–1348
20. Nagamatsu, S., Fujiwara, T., Nakamichi, Y., Watanabe, T., Katahira, H., Sawa, H., and Akagawa, K. (1996) *J. Biol. Chem.* **271,** 1160–1165
21. Ohara-Imaizumi, M., Nakamichi, Y., Tanaka, T., Ishida, H., and Nagamatsu, S. (2002) *J. Biol. Chem.* **277,** 3805–3808
22. Ohara-Imaizumi, M., Nishiwaki, C., Kikuta, T., Kumakura, K., Nakamichi, Y., and Nagamatsu, S. (2004) *J. Biol. Chem.* **279,** 8403–8408
23. Ohara-Imaizumi, M., Nishiwaki, T., Nakamichi, Y., C., Kikuta, Nagai S., and Nagamatsu, S. (2004) *Diabetologia*, in press
24. Ling, Z., Chen, M.-C., Smismans, A., Pavlovic, D., Schuit, F., Eizirik, D. L., and Pipeleers, D. G. (1998) *Endocrinology* **139,** 1540–1545
25. Chen, M-C., Schuit, F., and Eizirik, D. L. (1999) *Diabetologia* **39,** 875–890
26. Cardozo A. K., Heimberg, H., Heremans, Y., Leeman, R., Kutlu, B., Kruhoffer, M., Orntoft, T., and Eizirik D. L. (2001) *J. Biol. Chem.* **276,** 48879–48886
27. Rizzoli, S. O., and Betz, W. I. (2004) *Science* **303,** 2037–2039
28. Ling, Z., Van de Casteele, M., Eizirik, D. L., and Pipeleers D. G. (2000) *Diabetes* **49,** 340–345
29. Hoorens, A., Stange, G., Pavlovic, D., and Pipeleers, D. (2001) *Diabetes* **50,** 551–557
30. Washbourne, P., Thompson, P. M., Carta, M., Costa, E. T., Mathew, J. R., Lopey-Bendito, G., Molnar, Z., Becher, M. W., Valenzuela, C. F., Partridge, L. D., and Wilson. M. C. (2002) *Nat. Neurosci.* **5,** 19–26
31. Sorensen, J. B., Nagy, G., Varoqueaux, F., Nehring, R. B., Brose, N., Wilson, M. C., and Neher, E. (2003) *Cell* **114,** 75–86

Diabetologia (2004) 47:2200–2207
DOI 10.1007/s00125-004-1579-0

Diabetologia

Correlation of syntaxin-1 and SNAP-25 clusters with docking and fusion of insulin granules analysed by total internal reflection fluorescence microscopy

M. Ohara-Imaizumi[1] · C. Nishiwaki[1] · Y. Nakamichi[1] · T. Kikuta[1] · S. Nagai[1] · S. Nagamatsu[1]

[1] Department of Biochemistry, Kyorin University School of Medicine, Tokyo, Japan

Abstract

Aims/hypothesis. The interaction of syntaxin-1 and SNAP-25 with insulin exocytosis was examined using the diabetic Goto–Kakizaki (GK) rat and a total internal reflection fluorescence (TIRF) imaging system.
Methods. Primary rat pancreatic beta cells were immunostained with anti-syntaxin-1A, anti-SNAP-25 and anti-insulin antibodies, and then observed by TIRF microscopy. The real-time image of GFP-labelled insulin granules motion was monitored by TIRF.
Results. The number of syntaxin-1A and SNAP-25 clusters, and the number of docked insulin granules on the plasma membrane were reduced in GK beta cells. When GK rats were treated with daily insulin injection for 2 weeks, the number of syntaxin-1 and SNAP-25 clusters was restored, along with the number of docked insulin granules. The infection of GK beta cells with Adex1CA SNAP-25 increased the number of docked insulin granules. TIRF imaging analysis demonstrated that the decreased number of fusion events from previously docked insulin granules in GK beta cells was restored when the number of docked insulin granules increased by insulin treatment or Adex1CA SNAP-25 infection.
Conclusions/interpretation. There was a close correlation between the number of syntaxin-1 and SNAP-25 clusters and the number of docked insulin granules, which is associated with the fusion of insulin granules.

Keywords Diabetes mellitus · Evanescent · Exocytosis · Fusion · Insulin release · SNARE · TIRF

Introduction

The fundamental components of the secretory machinery required for the docking and fusion of vesicles with the plasma membrane have been revealed [1, 2]. These components, including *N*-ethylmaleimide-sensitive factor (NSF), soluble NSF attachment protein (SNAP), and membrane-associated SNAP receptors (SNAREs) such as syntaxin-1 and SNAP-25, are also expressed in pancreatic beta cells [3, 4, 5], which play an important role in insulin exocytosis [6, 7, 8, 9]. We [10] and others [11, 12] have demonstrated that the expression of SNARE proteins is decreased in diabetic animal models. It is conceivable that the expression of SNARE proteins is closely related to the docking/fusion of insulin exocytosis; however, there has been no apparent evidence to show the direct interaction between target membrane (t-)SNAREs and docking/fusion of insulin granules.

Imaging techniques are powerful tools for detecting vesicle trafficking and spatial distribution of membrane proteins in live cells and they have provided significant advances in understanding the mechanism of exocytosis [13, 14, 15]. In particular, the use of to-

Received: 10 May 2004 / Accepted: 5 August 2004
Published online: 11 December 2004

S. Nagamatsu (✉)
Department of Biochemistry,
Kyorin University School of Medicine, Mitaka,
Tokyo 181-8611, Japan
E-mail: shinya@kyorin-u.ac.jp
Tel.: +81-422-475511 ext 3437, Fax: +81-422-475538

Abbreviations: GFP, green fluorescent protein · GK, Goto–Kakizaki · NSF, *N*-ethylmaleimide-sensitive factor · SNAP, soluble NSF attachment protein · t-SNARE, target membrane SNAP receptor · TIRF, total internal reflection fluorescence

tal internal reflection fluorescence (TIRF) microscopy (also called evanescent wave microscopy), which allows fluorescence excitation within a closely restricted domain close to the plasma membrane (within 100 nm) [16], has permitted us to observe not only single granule movement underlying exocytosis [17, 18], but also the single molecules on the plasma membrane [19, 20]. Thus, we were able to observe using TIRF microscopy with high resolution, the single insulin granules approaching, docking, and fusing with the plasma membrane, and the spatial localisation of t-SNAREs such as syntaxin-1 and SNAP-25 in the plasma membrane of live cells.

In the present study, a TIRF system was utilised to address the question of whether t-SNAREs are related to the docking and fusion of insulin granules using insulin-treated and/or untreated diabetic Goto–Kakizaki (GK) beta cells where the expression levels of t-SNAREs and docking/fusion of insulin granules were changed. We demonstrate that t-SNAREs are closely associated with the number of docked insulin granules, in parallel with the fusion events from previously docked granules.

Materials and methods

Cells. Diabetic GK rats and non-diabetic male Wistar rats were obtained from a commercial breeder (Oriental Yeast, Tokyo, Japan). The rats were given free access to food and water until the start of experiments, which were conducted with 10-week-old male rats. The body weight of GK rats was not statistically different from that of controls. The plasma glucose concentration in the fed state, measured by the glucose oxidase method, was 12.3±0.78 mmol/l (n=16) in GK rats and 5.8±0.61 mmol/l (n=18) in control rats respectively (p<0.0001). For the normalisation of hyperglycaemia, human insulin (Humalin N; Lilly, Indianapolis, Ala., USA) was injected subcutaneously at 08.00 (2 U/rat) and 20.00 (4 U/rat) hours daily for 2 weeks. Pancreatic islets of Langerhans were isolated by collagenase digestion [10], with some modification. Isolated islets were dissociated into single cells by incubation in Ca^{2+}-free KRB containing 1 mmol/l EGTA, and cultured on fibronectin-coated (KOKEN, Tokyo, Japan) high-refractive-index glass (Olympus, Tokyo, Japan) in RPMI 1640 medium supplemented with 10% FBS (Invitrogen Gibco BRL, Carlsbad, Calif., USA), 200 U/ml penicillin, and 200 µg/ml streptomycin at 37 °C in an atmosphere of 5% CO_2.

Immunohistochemical analysis. Pancreatic beta cells were fixed, made permeable with 2% paraformaldehyde/0.1% Triton X-100, and processed for immunocytochemistry as described previously [9]. Cells were labelled with monoclonal anti-insulin antibodies (Sigma–Aldrich, St. Louis, Mo., USA), anti-HPC1-antibodies (Sigma-Aldrich), and anti-SNAP-25 antibodies (Wako, Osaka, Japan), and then processed with Cy3-conjugated anti-mouse IgG (Amersham Biosciences, Little Chalfont, UK). F-actin was stained by incubation with fluorescein isothiocyanate-conjugated phalloidin (Sigma-Aldrich). For double-immunostaining study, syntaxin-1 was stained with polyclonal anti-HPC-1-antiserum [5] and fluorescein anti-rabbit IgG (Jackson Immuno Research Laboratories, Bar Harbor, Me., USA). Immunofluorescence staining was detected by TIRF or epifluorescence microscopy.

TIRF microscopy. The Olympus total internal reflection system was used with minor modifications as described previously [18]. Light from an Ar laser (488 nm) or an He/Ne laser (543 nm) was introduced to an inverted epifluorescence microscope (IX70, Olympus) through a single-mode fibre and two illumination lenses; the light was focused at the back focal plane of a high-aperture objective lens (Apo 100× OHR; NA 1.65, Olympus). To observe the fluorescence image of Cy3, we

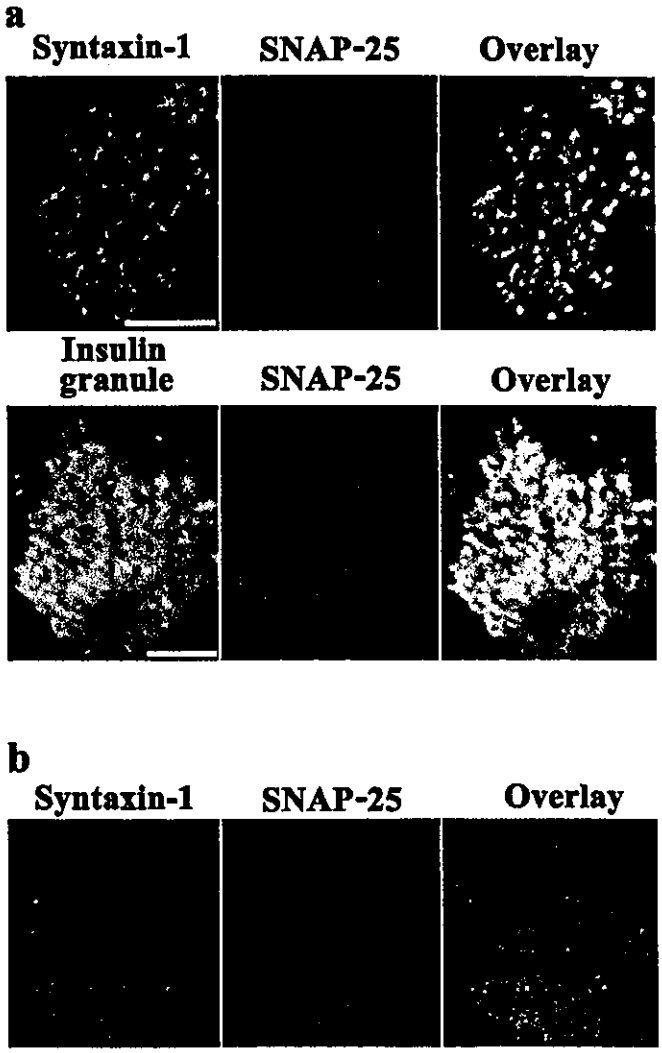

Fig. 1. SNAP-25 colocalised with syntaxin-1 and insulin granules on the plasma membrane of a primary rat pancreatic beta cell. **a.** TIRF images in a normal primary beta cell. After normal rat pancreatic beta cells were prepared, they were fixed, immunostained for syntaxin-1, SNAP-25 or insulin, and viewed simultaneously by TIRF microscopy as described [23]. The colocalisation of syntaxin-1 and SNAP-25, and of SNAP-25 and insulin granules is demonstrated by the superposition (yellow colour) of red and green channel images. **b.** TIRF image of SNAP-25-infected diabetic GK beta cell plasma membrane. Two days after GK beta cells were infected with Adex1CA SNAP-25, they were fixed, immunostained for syntaxin-1 and SNAP-25, and viewed by TIRF microscopy. The overlay of the images shows that most of the syntaxin-1 clusters were overlapped on SNAP-25 clusters

used a 543-nm laser line and a long-pass 590-nm filter. To observe green fluorescent protein (GFP) or fluorescein, we used a 488-nm laser line for excitation and a 515-nm pass filter for the barrier. The procedure for monitoring the GFP-labelled insulin granule motion in primary rat pancreatic beta cells is described elsewhere [21]. Briefly, primary beta cells expressing insulin–GFP on the glass cover slip (Olympus) were mounted in an open chamber and then transferred to the thermostat-controlled stage (37 °C). Cells were stimulated by 22 mmol/l glucose (final), and the measured penetration depths were about 45 nm.

Preparation of recombinant adenoviruses and adenovirus-mediated gene transduction. The construction of expression vectors and recombinant adenovirus encoding insulin–GFP and SNAP-25 has been previously described [10, 21]. To label

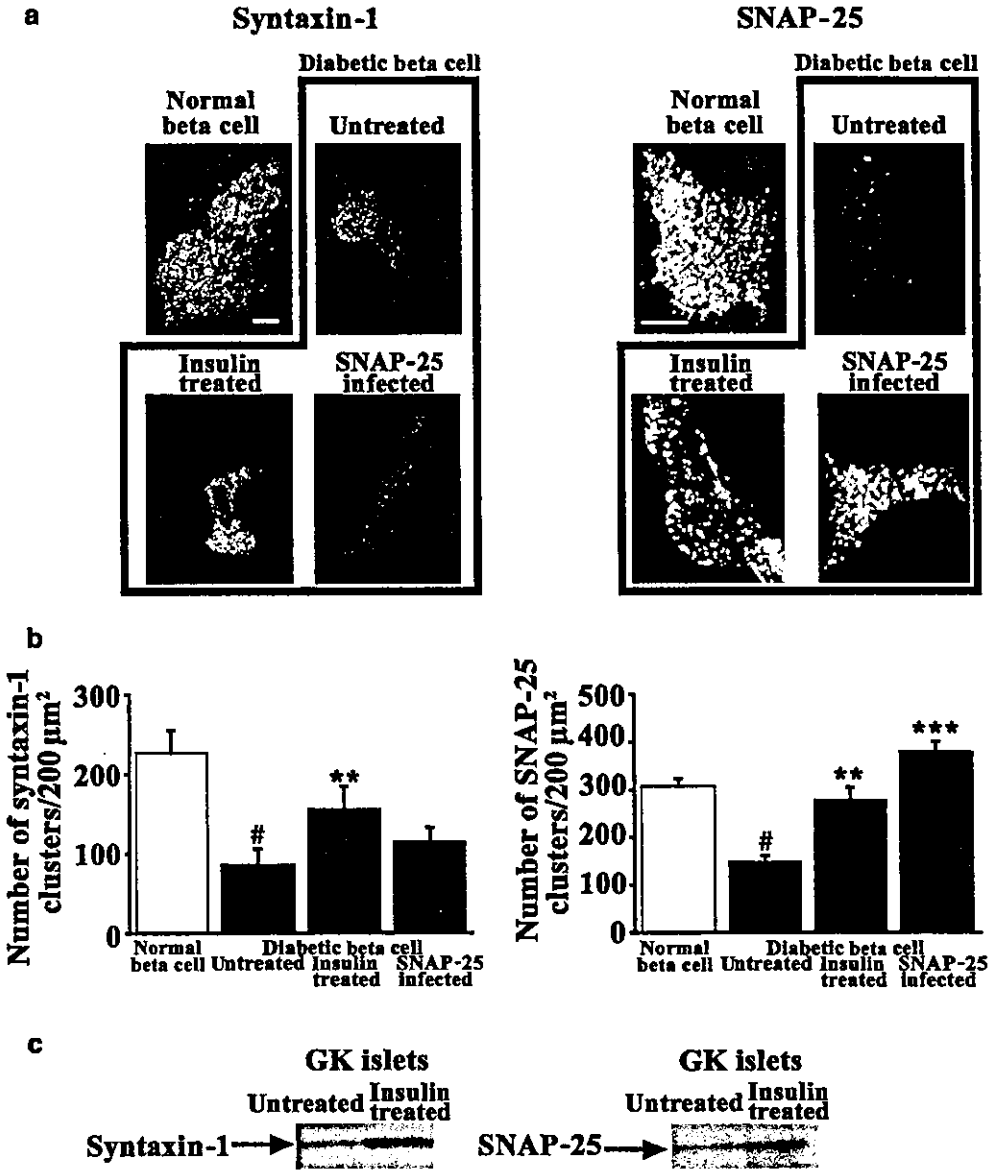

Fig. 2. TIRF images, and the immunoblot analysis of syntaxin-1 and SNAP-25 in normal and diabetic GK beta cells. **a.** Effects of insulin treatment and Adex1CA SNAP-25 infection on syntaxin-1 and SNAP-25 on the plasma membrane of diabetic GK beta cells were shown by TIRF images. Insulin-treated group: GK rats were treated with and/or without a daily subcutaneous injection of human insulin for 2 weeks, and then pancreatic beta cells were prepared. Adex1CA SNAP-25 infected group: the pancreatic beta cells prepared from GK rats were infected with Adex1CA SNAP-25 or Adex 1w (empty virus) and cultured for 2 days as described in Materials and methods. Treated GK or non-treated normal pancreatic beta cells were prepared and fixed, and then immunostained for syntaxin-1 and SNAP-25 before being observed by TIRF microscopy. The scale bars represent 5 μm. Each image is representative of separate experiments. **b.** The number of syntaxin-1 and SNAP-25 clusters in the plasma membrane. Individual fluorescent spots of syntaxin-1 and SNAP-25 shown in TIRF images were counted (normal beta cells, n=10; diabetic beta cells, n=8). The number of clusters was calculated per 200 μm². # $p<0.01$ vs normal, ** $p<0.01$ vs untreated, *** $p<0.001$ vs untreated beta cells. **c.** Immunoblot analysis. Islet proteins (200 islets) were extracted from insulin-treated and -untreated GK rat pancreas, subjected to SDS-PAGE, and immunoblotted with the indicated antibodies, which was followed by chemiluminescence reaction. Each immunoblot is a representation of three separate experiments. The levels of the protein bands were determined using the NIH Image program

the insulin secretory granules, cultured single cells were incubated with RPMI 1640 medium (5% FBS) and the required adenovirus (Adex1CA insulin–GFP, 30 MOI per cell) for 1 h at 37 °C, after which RPMI 1640 medium with 10% FBS was added. For SNAP-25 infection study, cultured single cells were infected with Adex1CA SNAP-25 (20 MOI per cell) prior to labelling the granules with Adex1CA insulin–GFP. Experiments were performed 2 days after the final infection.

Acquiring the images and analysis. Images were collected by a cooled charge-coupled-device camera (Micromax, MMX-512-BFT; Roper Scientific, Princeton Instruments, Trenton, N.J., USA) operated with Metamorph 4.6; Universal Imaging, Downingtown, Pa., USA) as described previously [21]. Most analyses, including counting the number of fluorescent spots, tracking (the single projection of different images) area calculations and fluorescent intensity, were performed using Metamorph software. To analyse the fusion data, fusion events were manually selected, and the average fluorescence intensity of individual granules in a 1-μm×1-μm square placed over the granule centre was calculated. The number of fusion events was manually counted while looping 15,000 frame time-lapses. TIRF images were finally exported as single TIFF files and were further processed using Adobe Photoshop 6.0.

Immunoblotting. Islets prepared from insulin-treated and/or insulin-untreated GK or normal Wistar rats were disrupted by sonication, boiled in SDS sample buffer with 10 mmol/l dithiothreitol, subjected to SDS-PAGE, and then transferred onto nitrocellulose filters. Immunoblotting procedures were performed as described previously [10] using anti-HPC-1-antibodies, anti-SNAP-25 antibodies, and anti-actin monoclonal antibody (Chemicon International, Temecula, Calif., USA). The protein bands were scanned and analysed by NIH Image.

Insulin release from islets. GK islets prepared before and after 2 weeks of daily insulin injection were preincubated with 2.2 mmol/l glucose in KRB for 1 h. They were then challenged with 22 mmol/l glucose plus forskolin (20 μmol/l). The media were collected at the end of the challenge period, then analysed for immunoreactive insulin by radioimmunoassay as previously described [9].

Statistical analysis. Results are means ± SEM, and statistical analysis was performed using ANOVA followed by Fisher's test and regression analysis using the Statview software (Abacus Concepts, Berkeley, Calif., USA).

Results

Decrease in the number of t-SNARE clusters and docked insulin granules in diabetic GK beta cell plasma membrane. A recent study using PC12 cells reported that t-SNAREs are concentrated in separate clusters, shown using membrane–sheet procedures [22]. Consistent with their results, we previously observed, using TIRF microscopy, that t-SNAREs are distributed in numerous spots in the MIN6 cell plasma membrane [23]. In the present study we examined this issue using rat primary pancreatic beta cells. As shown in Fig. 1a, the immunofluorescence of syntaxin-1 and SNAP-25 on the plasma membrane of rat primary pancreatic beta cells was distributed in numerous spots as well as in those observed in MIN6 cells.

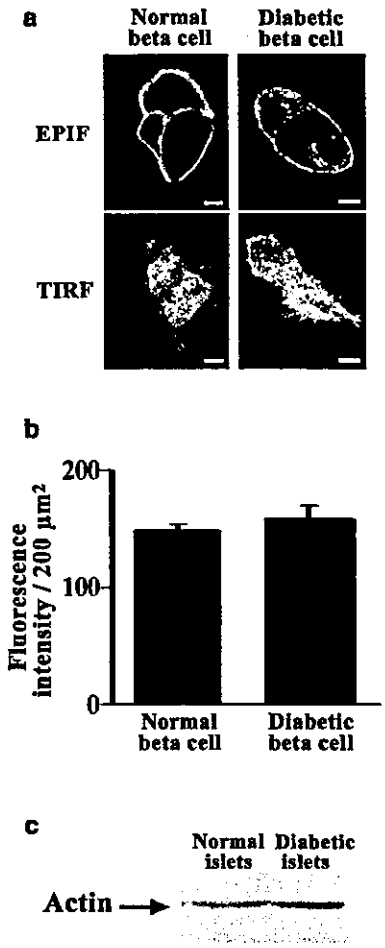

Fig. 3. Immunohistochemistry and immunoblot of actin in normal and diabetic GK beta cells. **a.** TIRF and epifluorescence (EPIF) images of F-actin on the beta cell plasma membrane. After pancreatic beta cells were prepared from normal and GK rat pancreas, F-actin was stained with phalloidin–fluorescein isothiocyanate and observed by TIRF and EPIF microscopy. Each image is representative of three separate experiments. **b.** The fluorescence intensity of phalloidin–fluorescein isothiocyanate analysed by Metamorph based on TIRF image (n=5 cells). **c.** Immunoblot analysis. Islet proteins were subjected to SDS-PAGE, immunoblotted with anti-actin monoclonal antibody, and scanned as described in the legend of Fig. 2 (n=3 for separate experiments)

The apparent diameters of the syntaxin-1 and SNAP-25 clusters were approximately 400 nm, which is similar to that reported in MIN6 cells [23]. Dual-stained immunohistochemical studies for syntaxin-1 and SNAP-25 showed that most of the syntaxin-1 clusters were colocalised with the SNAP-25 clusters, which were also colocalised with insulin granules docked on the plasma membrane (Fig. 1a). Thus, the characterisation of t-SNAREs on the plasma membrane appears not to be different between insulinoma MIN6 cells and primary pancreatic beta cells. We then examined the change of t-SNARE clusters in diabetic GK beta cells. In diabetic GK beta cells, TIRF images and their analyses showed that the number of clusters of syntaxin-1A and SNAP-25 decreased to less than half of that in

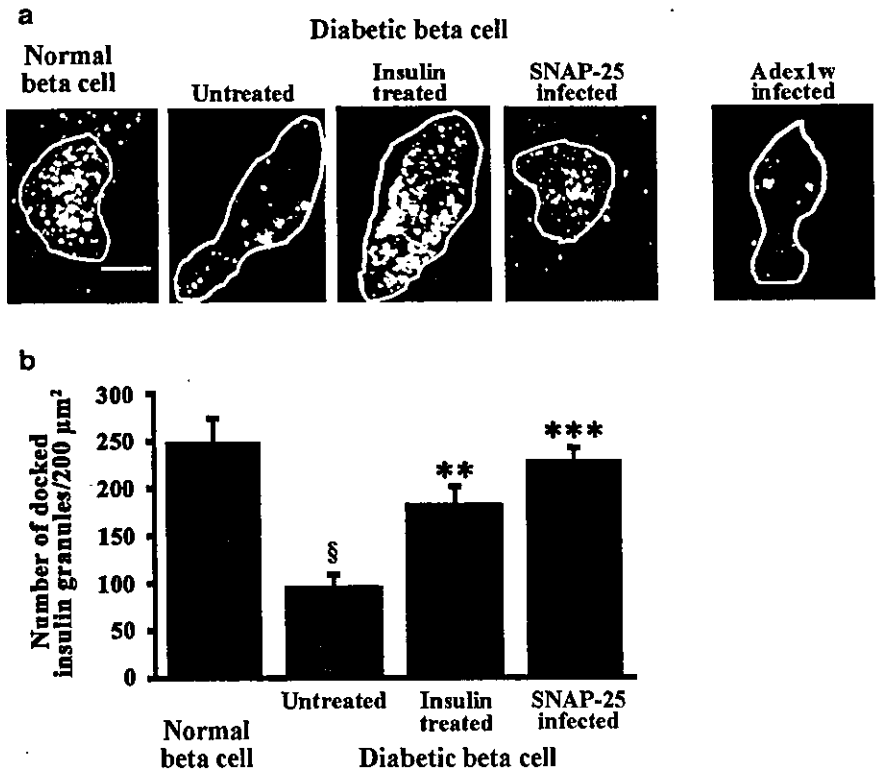

Fig. 4. Histochemical study of insulin secretory granules docked to the plasma membrane. **a.** TIRF images of docked insulin granules in normal and diabetic GK beta cells. For insulin treatment and Adex1CA SNAP-25 or Adex1w infection, GK rats and beta cells were processed as described in the legend of Fig. 2. Cells were fixed with paraformaldehyde, then immunostained for insulin. The surrounding lines represent the outline of cells that are attached to the cover glass. Representative images are shown. The scale bar represents 5 μm. Note that infection with Adex1w empty virus did not affect the docked insulin granules. **b.** The number of insulin granules morphologically docked to the plasma membrane. Individual fluorescent spots shown as TIRF images were counted and calculated per 200 μm² (normal beta cells, n=15; GK beta cells, n=8). § $p<0.0001$ vs normal beta cells, ** $p<0.01$ vs untreated diabetic beta cells, *** $p<0.001$ vs untreated diabetic beta cells

normal beta cells (Fig. 2a, b). To examine whether the decreased number of t-SNARE clusters in diabetic beta cells is a specific phenomenon, we immunostained F-actin as a control. As shown in Fig. 3, no differences in ring-shaped F-actin immunostaining or actin immunoblotting were observed between normal and diabetic beta cells, indicating that the alteration in the number of t-SNARE clusters in the diabetic GK beta cell is a specific phenomenon. Although actin signals in GK islets detected by immunoblot had a tendency to increase, no statistically significant difference was found between normal and GK diabetic islets by scanning and analysis of protein bands with NIH Image (100% vs 148±39%; n=3).

We then examined the change in insulin granules morphologically docked to the plasma membrane in diabetic GK beta cells. There is no precise definition of "morphologically docked granules", but the following are generally used: (i) vesicle is located within 200 nm of the plasma membrane, shown by electron microscopy [24]; (ii) vesicle is located within 100 nm of the surface membrane, shown by electron microscopy [25]; (iii) vesicle distance from plasma membrane is less than 10 nm, shown by TIRF microscopy [26]; and (iv) vesicle is in direct contact with the plasma membrane, shown by electron microscopy [27]. As the penetration depth under our TIRF condition is 80 nm, we defined "morphologically docked granules" as the vesicle being located within 100 nm of the plasma membrane. As shown in Fig. 4a, TIRF imaging depicted the single insulin granules morphologically docked to the plasma membrane, whereby we could manually count the number of docked insulin granules in normal and diabetic beta cells. As shown in Fig. 4b, the number of insulin granules docked to the plasma membrane was markedly reduced in diabetic GK beta cells.

Recovery of the number of t-SNARE clusters and docked insulin granules by insulin treatment. We addressed the question of whether the normalisation of blood glucose levels affects the number of t-SNARE clusters and the number of docked insulin granules in GK beta cells. We treated GK rats with daily insulin injection for 2 weeks, resulting in the reduced blood glucose levels (untreated 11.2±0.61 vs treated 5.6±0.33 mmol/l). After 2 weeks of insulin treatment, pancreatic beta cells were prepared and immunostained with anti-syntaxin-1A, anti-SNAP-25, and anti-insulin antibodies. The number of syntaxin-1 and

SNAP-25 clusters in the plasma membrane was partially, but significantly, recovered to subnormal levels (Fig. 2a, b). Immunoblot analysis also showed that the levels of syntaxin-1A and SNAP-25 were increased in islets isolated from insulin-treated GK rats (Fig. 2c; 182±24% in syntaxin-1, 165±32% in SNAP-25 when expressed as 100% in insulin-untreated GK islets, n=3 for each, p<0.01). It is of note that along with an increase in the number of t-SNARE clusters, there was also an increase of about two-fold in the number of insulin granules docked to the plasma membrane (Fig. 4a, b).

Correlation between the fusion events and the number of docked insulin granules. We previously reported that the fusion events during first-phase release originate from previously docked granules (resident) both in MIN6 cells and primary pancreatic beta cells [18, 21]. In the present study, we tested whether the number of fusion events is correlated with the number of docked insulin granules. After pancreatic beta cells were prepared from normal rats, insulin-untreated and insulin-treated GK rats, they were infected with Adex1CA insulin–GFP to label the insulin secretory granules. After 2 days of infection, granule motion was monitored using TIRF by 22 mmol/l glucose stimulation. In insulin-untreated diabetic GK beta cells, the fusion events from previously docked granules were rarely observed (Fig. 5; untreated). In contrast, in insulin-treated GK beta cells, high glucose stimulation caused fusion events from previously docked insulin granules (Fig. 5; treated) where the number of docked insulin granules was recovered to subnormal levels (see Fig. 4). Furthermore, we measured insulin release from GK islets before and after insulin treatment. Consistent with the results of the TIRF imaging analysis, glucose-stimulated insulin release from insulin-treated GK islets was slightly improved compared with before treatment (1.5±0.3 ng·islet^{-1}·h^{-1} before treatment vs 2.1±0.4 ng islet^{-1}·h^{-1} after treatment, p<0.01, n=3 for separate experiments).

Rescue of fusion events by recovering the number of docked insulin granules and restoring SNAP-25 clusters to normal levels. In order to examine whether the concentration of t-SNARE clusters is linked to the docking status followed by subsequent fusion of insulin granules, we restored the decreased number of SNAP-25 clusters to normal levels by infecting GK beta cells with Adex1CA SNAP-25. GK beta cells infected with Adex1CA SNAP-25 showed the normalised number of SNAP-25 clusters on the plasma membrane (Fig. 2a, b) where the decreased number of docked insulin granules was also restored to subnormal levels (Fig. 4). However, infection with Adex1CA SNAP-25 did not affect the number of syntaxin-1 clusters (Fig. 2a). GK beta cells infected with empty

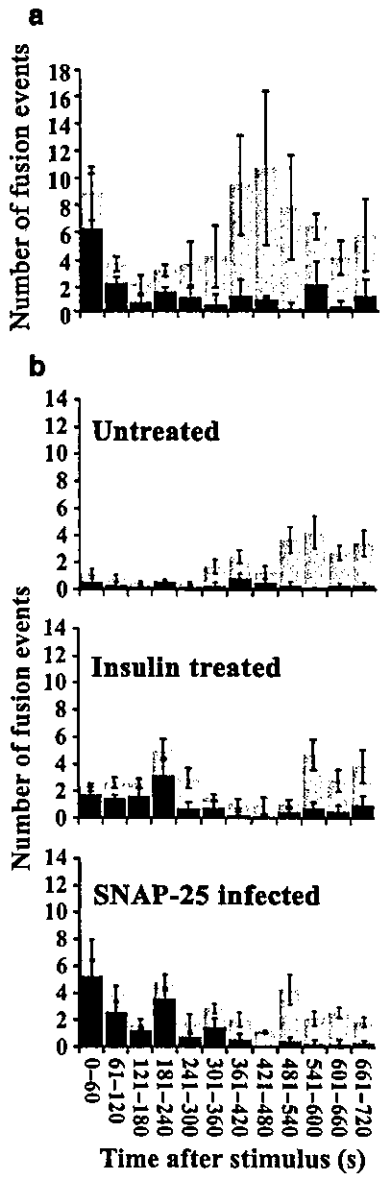

Fig. 5. Restoration of the decreased number of fusion events in normal (**a**) and diabetic (**b**) beta cells. Black bars, resident; grey bars, newcomer. For insulin treatment and SNAP-25 infection, GK beta cells were prepared as in the legend of Fig. 2. After these procedures, beta cells were infected with Adex1CA insulin–GFP in order to label the insulin granules, then the real-time motion of GFP-labelled insulin granules during stimulation with 22 mmol/l glucose was imaged close to the plasma membrane by TIRF, and fusion was analysed by Metamorph software. The graph shows the histogram of the number of fusion events (per 200 μm^2; normal beta cells, n=5; GK beta cells, n=4)

virus Adex 1w did not show any change in the number of SNAP-25 clusters (data not shown) or in the number of docked insulin granules (Fig. 3a). As shown in Fig. 1b, most of the syntaxin-1 clusters were colocalised with SNAP-25 clusters restored by Adex1CA SNAP-25 infection in GK beta cells. Cotransfection of Adex1CA SNAP-25 with Adex1CA syntaxin-1A did not affect the subnormalised number of docked insulin

granules (data not shown). We then performed TIRF imaging analysis of the docking and fusion of insulin granules stimulated by 22 mmol/l glucose using Adex1CA-SNAP-25-infected GK beta cells. These beta cells showed a marked increase in fusion events from previously docked granules (Fig. 5; SNAP-25 infected).

Discussion

In the present study, we examined the interaction between the number of t-SNAREs and the number of insulin granules docked to the plasma membrane, and between the number of docked insulin granules and the number of fusion events. Our data demonstrated a close correlation of t-SNARE clusters with docked insulin granules, and that the number of docked insulin granules was correlated with the fusion events from previously docked granules.

TIRF imaging showed that the number of syntaxin-1A and SNAP-25 clusters and the number of docked insulin granules on the plasma membrane decreased in GK beta cells. It is of note that the recovery of the decreased number of SNAP-25 clusters in GK beta cells to normal levels by adenovirus treatment or insulin treatment could restore the number of docked insulin granules, which caused an increased number of fusion events from previously docked granules. We previously reported that restoration of decreased t-SNARE levels improved the impaired insulin secretion in GK islets [10]. At that time, however, we could not know how t-SNARE restoration affects the insulin exocytosis. Now, we know that the restored number of SNAP-25 clusters subnormalised the number of docked insulin granules, through which the fusion from previously docked granules was probably recovered. Thus, in diabetic GK beta cells, the decreased number of t-SNARE clusters may result in impaired insulin granule docking status followed by a decreased fusion event that might lead to the loss of first-phase insulin release. We have recently reported that the disruption of t-SNARE clusters by cholesterol depletion with methyl-β-cyclodextrin treatment causes the inhibition of docking and fusion of insulin granules [23] and thus indicates that impaired formation of t-SNARE clusters in diabetic GK beta cells may be involved in the decreased docking and fusion events of insulin granules.

It is interesting that the transduction with Adex1CA SNAP-25 alone was sufficient to recover the reduced number of docked insulin granules in diabetic GK beta cells, which was followed by an increase in fusion events. Indeed, we had found that the transduction of GK islets with Adex1CA SNAP-25 alone recovered the glucose-stimulated insulin release effectively [10]. Although the precise reason why the restoration of SNAP-25 clusters alone recovered the impaired docking and fusion events in spite of the imbalance in relative levels of SNAP-25 and syntaxin-1 is not known at present, SNAP-25 may be a strict requirement more so than syntaxin-1 in evoked fusion event, as recently shown [28, 29]. Further studies about this important issue are required.

The present study also reported the interesting finding that insulin treatment improved the impaired docking and fusion events in GK beta cells. Although one clinical study showed that the impaired insulin release in diabetic patients was improved when the hyperglycaemia was normalised by daily insulin injection [30], there have been no in vitro studies to examine its mechanism in detail. Judging from our data, it is conceivable that insulin treatment may have reduced the insulin secretion and thus allowed beta cells to increase the number of docked granules. However, because the effects of insulin treatment persisted for at least 2 days during culture period after beta cell preparation, these would be trophic effects. Another simple explanation would be that improved glucotoxicity by insulin treatment may have recovered the beta cell functions.

Finally, we calculated the total number of docked insulin granules in rat pancreatic beta cells. On the basis of our data, we estimated that normal primary beta cells contain approximately 1200 insulin granules docked to the plasma membrane. As the surface area of a beta cell is reported to be 973 μm^2 [31] and the number of docked granules of normal beta cells is calculated to be 246 granules/200 μm^2, the total number of docked insulin granules is about 1200. In a study that used mouse pancreas and electron microscopy [31], Dean reported that the pancreatic beta cells contain about 13,000 insulin granules, and recently, mouse and rat beta cells were reported to have about 10,000 insulin granules per cell, with an estimated number of docked granules of about 600 and 450 respectively [32, 33]. Thus, the number of docked insulin granules is slightly larger in our TIRF imaging analysis. The discrepancy may be because (i) electron microscopy only provides a snapshot of the situation in the beta cells at the time of fixation, so it is not possible to conclude that a certain number of docked granules are really physically attached to the plasma membrane; or (ii) TIRF imaging only gives information on a small part of the cell attached to the coverglass where vesicles are located within 100 nm of the plasma membrane, so the calculated total number of granules docked to the whole cell surface may be an overestimation.

In conclusion, there was an interaction between the number of t-SNARE clusters and the number of docked insulin granules, which were associated with fusion events from previously docked insulin granules.

Acknowledgements. We thank I. Saito for kindly providing the adenovirus cosmid vector and parental virus. This work was supported by Grants-in-Aid for Scientific Research (C)